Structure- and Sampling-Adaptive Gait Balance Symmetry Estimation Using Footstep-Induced Structural Floor Vibrations

Jonathon Fagert, P.E., S.M.ASCE[1]; Mostafa Mirshekari, A.M.ASCE[2]; Shijia Pan[3]; Linda Lowes[4]; Megan Iammarino[5]; Pei Zhang[6]; and Hae Young Noh, A.M.ASCE[7]

Abstract: This paper presents a structure- and sampling-adaptive approach for analyzing human footstep-induced structural floor vibrations to estimate footstep ground reaction forces (GRFs) and gait balance symmetry. Balance symmetry and footstep GRFs are critical indicators of overall gait health and elderly fall risks. Prior works, including direct observation by trained medical personnel, computer vision-, pressure sensor-, and wearable-based sensing, are limited due to operational restrictions. We introduce a nonintrusive balance symmetry monitoring approach, which utilizes sparse structural vibration sensing. The intuition is that footstep-induced floor vibration responses are proportional to footstep GRFs, and balance symmetry can be defined using consecutive GRF pairs. However, GRF-vibration relationships are also influenced by spatially-varying structural properties and gait sampling bias, introducing errors to real-world estimations. We address these challenges first by extracting structural regions to overcome spatially-varying vibration behavior and then by developing a kernel-based robust regression model to overcome biased training data and enable robust GRF and balance symmetry modeling. We evaluate our approach through real-world experiments, achieving a balance symmetry index estimation accuracy as high as 96.5%. **DOI: 10.1061/(ASCE)EM.1943-7889.0001889.** © *2020 American Society of Civil Engineers.*

Introduction

Gait balance symmetry assessment and footstep ground reaction force estimation are important for understanding occupants' overall gait health. In the context of gait health, balance symmetry refers to a person's ability to maintain their center of mass between their left- and right-feet. Specifically, in this work, balance is considered to be the difference between consecutive left- and right-foot walking ground reaction forces (GRFs). Balance symmetry information has been shown to be a critical aspect of fall prediction in elderly populations (Rubenstein 2006; Lord et al. 2003; Nevitt et al. 1989; Shupert and Horak 2016; Vaught 2001; Perell et al. 2001), as well as diagnosing gait disorders (Horak 1997) and various neurological/musculoskeletal conditions (Aruin and Kanekar 2013). As a result, frequent measurements of balance symmetry (i.e., in home-settings and assisted-living settings) can help individuals understand their overall health and safety risks and lead to improvements in the quality of life.

Prior methods for assessing gait balance symmetry include direct observation by medical staff (Pardasaney et al. 2012; Mancini and Horak 2010; Karuka et al. 2011), pressure/force-based sensing, vision-based sensing, and wearable-based sensing (Mancini and Horak 2010; Karuka et al. 2011; Kamen et al. 1998; Browne and O'Hare 2001). These existing approaches are widely accepted by medical professionals and can achieve high accuracy for estimating balance symmetry but have operational limitations [e.g., dense sensor deployment (pressure/force sensors), line of sight (vision), and requiring users to carry a device (wearables)] that prevent them from widespread use in nonclinical settings. The "Related Work" section explores these existing approaches in more detail.

A recent approach to measuring gait health is to use structural floor vibrations (Lam et al. 2016; Fagert et al. 2017a, 2019a, b, 2020; Kessler et al. 2019). These approaches rely on the physical interaction between footsteps and the underlying building structure to estimate spatiotemporal gait characteristics and other human information (e.g., step frequency, stride length, step time, and person identification). The benefits of using structural floor vibrations are that gait information can be collected passively, with sparse sensing [up to a 20-m sensing range (Pan et al. 2017b)] and without requiring the persons walking to wear or carry a device. However, these prior works focus on high-level gait information (e.g., step frequency, stride length, and so forth) and do not account for human walking behaviors or spatially-varying structural behavior. As such, they cannot accurately extract fine-grained gait information, such as ground reaction forces and balance symmetry.

[1]Ph.D. Candidate, Dept. of Civil and Environmental Engineering, Carnegie Mellon Univ., 5000 Forbes Ave., Pittsburgh, PA 15213 (corresponding author). Email: jfagert@cmu.edu

[2]Postdoctoral Researcher, Dept. of Civil and Environmental Engineering, Stanford Univ., Y2E2, 473 Via Ortega, Stanford, CA 94305. Email: mmirshek@stanford.edu

[3]Assistant Professor, Dept. of Computer Science and Engineering, Univ. of California, Merced, 5200 North Lake Rd., Merced, CA 95343. Email: span24@ucmerced.edu

[4]Principal Investigator, Abigail Wexner Research Institute at Nationwide Children's Hospital, 700 Children's Dr., Columbus, OH 43205. Email: Linda.Lowes@nationwidechildrens.org

[5]Research Physical Therapist, Abigail Wexner Research Institute at Nationwide Children's Hospital, 700 Children's Dr., Columbus, OH 43205. ORCID: https://orcid.org/0000-0003-2800-3855. Email: Megan.Iammarino@nationwidechildrens.org

[6]Associate Research Professor, Dept. of Electrical and Computer Engineering, NASA Research Park, Carnegie Mellon Univ., P.O. Box 98, Moffett Field, CA 94035. Email: peizhang@cmu.edu

[7]Associate Professor, Dept. of Civil and Environmental Engineering, Stanford Univ., Y2E2, 473 Via Ortega, Stanford, CA 94305. Email: noh@stanford.edu

Note. This manuscript was submitted on May 18, 2020; approved on September 14, 2020; published online on December 15, 2020. Discussion period open until May 15, 2021; separate discussions must be submitted for individual papers. This paper is part of the ***Journal of Engineering Mechanics***, © ASCE, ISSN 0733-9399.

To extract footstep ground reaction force and balance symmetry information, this work uses the insight that the amplitudes of the structural floor vibrations are directly influenced by and proportional to the magnitudes of the footstep ground reaction forces. However, in real-world applications, the relationship between measured floor vibration signals and footstep GRFs is affected by spatial variations in the structural characteristics (e.g., damping, stiffness, and mass) of the underlying structure (a.k.a., the *structural variation effect*) (Pai et al. 2019; Drira et al. 2019). Further, healthy humans tend to walk similarly across different steps (Pan et al. 2017c), resulting in a narrow range of GRFs for training and failure to capture behavior in the *extreme* regions (i.e., unbalanced gait). Collecting training data from these extreme regions is difficult because most data sources are persons with gait abnormalities, injuries, and/or elderly persons—it is not reasonable to ask one's grandparent to walk a hundred times down a hallway. As a result, this *gait sampling bias* results in a model bias toward the middle range of GRFs and an erroneous estimation of the extreme GRFs. The combination of these two effects makes it challenging to estimate footstep GRFs and balance symmetry from the raw vibration signal alone and introduce significant modeling errors.

This paper presents a structure- and sampling-adaptive approach for estimating footstep GRFs and gait balance symmetry. To the best of our knowledge, this is the first work to leverage footstep-induced structural vibrations for individualized GRF and balance estimation. Specifically, we measure the amplitude of footstep-induced structural vibrations and model the relationship between this amplitude and footstep GRFs. The *structural variation effect* on the vibration signal is addressed by isolating the structural components of the footstep responses and clustering them into spatial structural regions throughout the sensing area through a principal component projection of their frequency responses. By isolating the effects of the structural regions and their respective attenuation rates, our method is able to directly observe the changes in vibration responses due to variations in footstep GRFs. Then, to overcome model bias due to limitations in data distribution across the full footstep GRF range (the *gait sampling bias*), we train our GRF-amplitude models using a kernel-based robust regression. The weights for the regression model are designed using an inverse probability density function of the training data, which allows us to place more weight on the extreme GRFs and reduce the model bias. This approach enables accurate GRF and balance symmetry estimation with less training data and reduces the influence of a narrow GRF range on the GRF-vibration amplitude model. We validate our approach through real-world deployments in three types of structures (wood-framed, steel-framed, and concrete slab-on-grade) and with six different persons walking.

The remaining sections of the paper are organized in the following way. The "Related Work" section discusses related work on current approaches for GRF, balance estimation, and load identification, as well as their limitations. Next, we present the physical insight that enables our force and balance estimation approach. Then, we provide a detailed description of our approach. Next, the results of our experimental validation are presented with different structures and several walking participants. Finally, we discuss directions for future work and summarize our work and its potential for enabling gait analysis and smart healthcare in nonclinical settings.

Related Work

In this work, we utilize footstep-induced floor vibrations to obtain estimates of footstep ground reaction forces and use those to estimate gait balance symmetry. As previously discussed in the section "Introduction," much of the prior work in this field can be placed in two categories: (1) direct observation-based approaches and (2) sensing-based approaches. In the next section, we discuss each of these categories in more detail and address how our work fills the research gap that exists with prior approaches. In addition, our treatment of structural floor vibrations to obtain force estimations can be viewed as a load identification problem in structural dynamics. We discuss prior works in this domain in the "Vibration Load Identification" section.

Gait Balance Symmetry and Ground Reaction Force Sensing Approaches

Gait balance symmetry is a common component of clinical gait assessment. Because of its ubiquity, the study of gait balance symmetry is a broad field in biomechanics. Studies in this area typically focus on extracting dynamic gait balance parameters, such as symmetry index (SI), the center of pressure (CoP), the center of mass (CoM), and extrapolated center of mass (XCoM) (Herzog et al. 1989; Lugade et al. 2011; Lugade and Kaufman 2014; Hof et al. 2005; Gutierrez-Farewik et al. 2006; van Meulen et al. 2016a). For each of these metrics, the primary objective is to quantify how the body moves from one side to the other while walking. By studying this effect, it is possible to understand walking instabilities, which can be associated with underlying conditions/disorders (e.g., stroke, knee/hip problems, and so forth), or with fall risks in elderly populations (Rubenstein 2006; Lord et al. 2003; Nevitt et al. 1989; Shupert and Horak 2016; Vaught 2001; Perell et al. 2001; Horak 1997; Aruin and Kanekar 2013). In this work, we focus on quantifying gait balance by estimating vertical footstep ground reaction forces (GRFs) and using consecutive pairs of GRFs to calculate gait balance using the symmetry index metric. Further details regarding how this metric is obtained are discussed in the "Clustered Kernel-Based Learning" section.

Traditionally, the most common technique used for gait balance symmetry assessment is a direct observation by trained medical personnel. However, this approach is typically limited to qualitative measurements using tests such as the Timed Up and Go test, the Dynamic Gait Index, and the Tinetti Balance and Gait test (Pardasaney et al. 2012; Mancini and Horak 2010; Karuka et al. 2011; van Meulen et al. 2016b; Berg et al. 1989; Mathias et al. 1986; Shumway-Cook and Woollacott 1995; Jonsdottir and Cattaneo 2007). In addition, this approach requires gait assessment to be performed in clinical settings; as a result, changes in gait and balance may not be captured with sufficient temporal resolution to monitor fall risks for elderly populations, changes in gait associated with neurodegenerative conditions (e.g., cerebral palsy), or gait impairments, such as hip or knee joint failure.

To address the limitations of the direct observation approach, numerous sensing-based approaches have emerged. One approach, which uses vision-based sensing combined with computer vision algorithms, tracks the movement of the body while walking (Muro-de-la Herran et al. 2014; Benedetti et al. 1999; Xue et al. 2010; Gabel et al. 2012). However, this approach is limited to scenarios in which a direct line-of-sight is possible, so gait balance assessment cannot be conducted if walls, furniture, and other persons occlude the view of the sensing system. Additionally, vision-based sensing in certain environments (e.g., bathrooms and bedrooms) raises concerns of perceived privacy, therefore limiting its deployment in nonclinical settings.

Another sensing-based approach uses pressure/force sensing. For these systems, the sensors directly measure the footstep ground reaction forces and use these measurements to assess gait balance symmetry (Wafai et al. 2015; Wearing et al. 2001; Lord et al. 1986;

McDonough et al. 2001). In order to achieve high fidelity in GRF estimation and gait balance assessment, these approaches require a sensor in every location that a footstep may occur. For nonclinical settings, this dense sensor deployment requirement quickly becomes impractical as sensing mats would be required to be placed in every habitable area of a building, which is both expensive and difficult to deploy/maintain.

Wearable-based sensing is another indirect approach for estimating gait balance symmetry. With this approach, pedestrians are required to wear or carry a device, such as an accelerometer or other inertial-based sensor, and gait balance symmetry is inferred through the recorded motion of the sensor (Kamen et al. 1998; Tien et al. 2010; Spain et al. 2012). These approaches overcome the limitations of other methods in that they enable continuous monitoring of gait balance symmetry outside of clinical settings but are limited by the need for the user always to wear or carry a device. In scenarios such as elder care, this requirement may limit their use and appeal. Further, some recent studies have shown that more than half of individuals who own a wearable device stop using it, and many of them do so within 6 months of ownership (Patel et al. 2015).

By utilizing footstep-induced structural floor vibrations, our method overcomes the limitations of these existing sensing approaches. Through leveraging vibration wave propagation, our method enables sparse sensor deployment [we have observed a sensing range of up to 20 m (Pan et al. 2017b)], which can be retrofitted into any structure without any disruption to normal operations and daily activities. Their one-time installation can be done by placing the sensors directly on the existing floor of the building in the areas where monitoring is desired, and each low-cost sensor can monitor footsteps and human gait over a large area (as opposed to one sensor being required at each step location for pressure/force sensors). Further, this approach is not sensitive to visual obtrusion, has fewer perceived privacy concerns, and passively collects footstep and gait balance symmetry information without the need for users to carry a device. By removing the need for the user to interact with the sensing devices, our system enables more reliable around-the-clock monitoring of gait in nonclinical environments.

Prior works utilizing vibration sensing have achieved success in identifying (Pan et al. 2015, 2017c), tracking/detecting (Pan et al. 2016; Poston et al. 2017a; Pai et al. 2019; Drira et al. 2019; Madarshahian et al. 2016), localizing (Mirshekari et al. 2016, 2018b; Poston et al. 2017b; Alajlouni et al. 2018), and monitoring the activity of indoor occupants (Fagert et al. 2017b; Pan et al. 2017a, 2018, 2019; Bonde et al. 2020) and have also successfully estimated spatiotemporal gait parameters (Lam et al. 2016; Fagert et al. 2017a, 2019a, b, 2020; Kessler et al. 2019). However, these existing approaches do not account for the step-level variations in human walking resulting from the footstep ground reaction forces and underlying structural properties. By accounting for these characteristics, our method accurately estimates footstep ground reaction forces and gait balance symmetry.

Vibration Load Identification

Load identification in structural dynamics addresses the inverse problem in which a structural vibration response is known, but the input excitation/force is not known. Much of the prior work in this domain is focused on pedestrian load identification with respect to the impact on structural behavior. In this way, these works focus on modeling pedestrian footstep-induced loads as periodic excitations to the structure to understand structural responses to impulsive loads. These works primarily involve four areas: (1) leveraging a finite-element model or modal information to solve the inverse load identification problem (Law 2002; Willford et al. 2006; Racic et al. 2009); (2) utilizing artificial neural networks (ANNs) or other deep-learning approaches to establish force transfer functions (Cao et al. 1998); (3) output-only methods that estimate modal parameters of the structure to estimate the frequency response function and forcing functions through inverse modeling and developing simplified structure models (Shahabpoor et al. 2016; Pimentel et al. 2001); and (4) statistical-based load models that assume harmonic loading based on weight-based footstep force models (Racic and Brownjohn 2011; Živanović et al. 2007). For real-world buildings, prior information about the structural dynamic properties is either not known or not easy to obtain. As a result, the inverse modeling approach of these existing works may not be able to estimate footstep force-induced vibrations and, subsequently, gait balance symmetry. In addition, other load identification problems are focused on obtaining a generic footstep forcing function in order to obtain information regarding structural performance. Therefore, these models typically assume a weight-normalized constant footstep forcing function, which does not take into account step-level variations in the footstep ground reaction forces due to changes in walking behavior or gait balance symmetry. On the other hand, our approach does not make any assumptions about the underlying structure's dynamic properties and can accurately estimate individualized footstep GRFs and gait balance symmetry without any prior information about the structure.

Physical Insight: Footstep-Induced Floor Vibrations

To enable the footstep ground reaction force and balance symmetry estimation approach in this work, we utilize footstep-induced vibration wave propagation in floor structures. In this section, we provide an overview of the underlying physics that influence floor vibrations and discuss how we leverage physical insights regarding human gait and structural dynamics to overcome the challenges associated with our approach.

Human Gait Cycle and Ground Reaction Forces

Footstep-induced floor vibrations are fundamentally related to the physical interaction between footsteps, the floor, and the human gait cycle. In a typical gait, a pedestrian goes through several gait phases between each footstep. This work focuses on the three primary aspects of the stance phase: (1) the heelstrike transient (initial contact phase), (2) weight acceptance (loading response phase), and (3) toe push-off (Uustal and Baerga 2004). These phases represent when the foot strikes the floor, when the full body weight is supported by one foot, and when one foot transitions from the heel to the toe to facilitate forward motion and transition to the opposite foot.

We determine the temporal relationship between footstep GRFs and vibration responses by comparing the temporal characteristics of simultaneously collected GRF and vibration data. Fig. 1(a) shows an example of the footstep ground reaction forces collected from one of our experimental participants with shoe-mounted pressure sensors, which resembles the typical footstep GRF representation in the medical domain. The first peak represents the heelstrike transient, the second peak represents the weight acceptance, and the third peak represents the toe push-off. Note that the percent body weight (% BW) values shown (around 90% BW) are slightly less than typical values at the peak locations (>100% BW in most cases for the loading response peak), and the toe push-off peak is typically closer in magnitude to the loading response peak. This deviation in the figure shown is due to the practical limitations of the pressure sensors used. Due to the size of the sensors, we

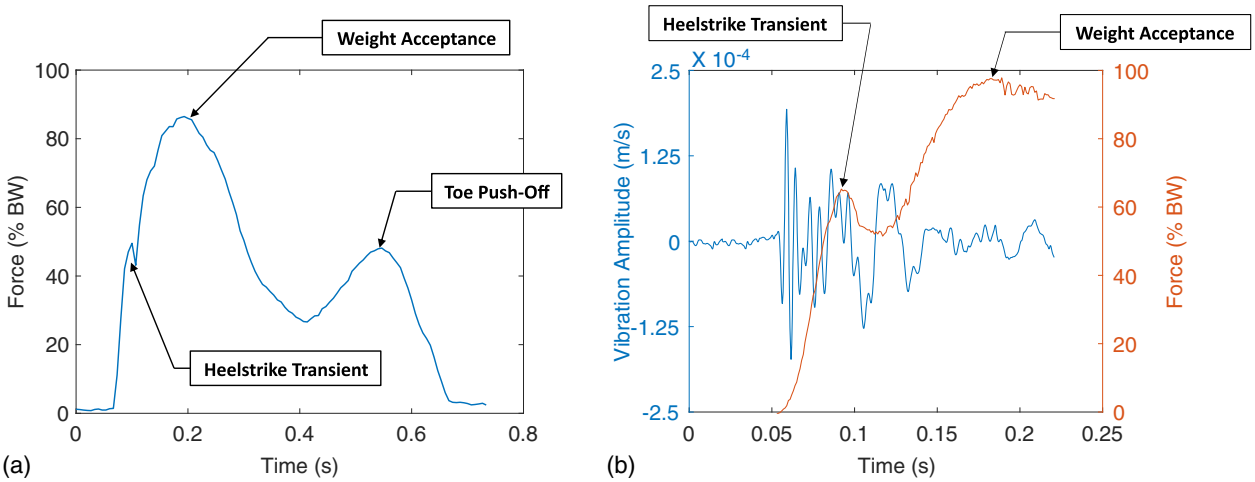

Fig. 1. (a) Example of footstep ground reaction forces collected using shoe-mounted pressure sensors. The first peak represents the heelstrike transient, while the second and third peaks represent weight acceptance and toe push-off, respectively; and (b) correlation between the heelstrike transient and the corresponding vibration signal. The majority of the vibration signal results from the application of the heelstrike transient force.

were not able to completely cover the sole of the shoe. As a result, the full magnitude of the GRFs was not captured, and in some instances, the data collected with our ground truth system did not achieve the typical peak GRF of 100% BW. However, for this study, we are focused on obtaining a measure of gait balance symmetry using a metric known as the symmetry index (SI) obtained using the peak heelstrike transient values (Herzog et al. 1989), so measuring the full 100% BW loading response peak is not necessary. We are choosing to use the peak heelstrike transient-values-based studies that have attributed the heelstrike transient to healthy walking and have identified it as the most demanding task in the gait cycle (Racic et al. 2009; Verdini et al. 2006). In this way, we concentrate pressure sensors on the heel of the shoe to ensure accurate measurement of the heelstrike transient ground reaction forces.

Using the GRF information from Fig. 1(a), we can determine which phases of the gait most strongly correlate with vibration responses. Fig. 1(b) shows an example of the collected GRF data and corresponding floor vibration signal. In this figure, we can make a few key observations: (1) as expected, the onset of the vibration signal occurs concurrently with the onset of the overall footstep GRF at 0.05 s; (2) the duration of the vibration response (from 0.05 to 0.15 s) is similar to the duration of the initial contact/heelstrike transient phase of the GRF (0.05 to 0.12 s), which is consistent with typical values in the medical literature (Whittle 1999); and (3) the vibration response has reduced/dampened to near ambient levels at the time of later gait phases (i.e., the weight acceptance phase at around 0.2 s). As such, there is an indication that the vibration response and the initial contact/heelstrike transient phase of the GRF are the most directly related, and consequently, the peak vibration response is primarily generated from the peak heelstrike transient. While this example shows just one instance of the timing of the heelstrike transient/initial contact gait phase and the vibration response, our observation is that this represents the general relationship, and the vibration response rarely exceeds the duration shown. Additionally, even in cases of structures with low damping/stiffness (in which the vibration signal tends to have a longer duration), the primary reason for the longer signal is that the free vibration is longer (i.e., the vibration response after the application of the force has terminated). Based on these observations, the system in this work defines the output GRF as the peak amplitude of the heelstrike transient phase of the footstep ground reaction force.

Footstep-Induced Structural Vibration Dynamics

In our approach, we model the vibration response as the output of a linear time-invariant system subjected to a time-dependent forcing function (the footstep GRF). We monitor the vertical component of footstep-induced floor vibrations only because the majority of the footstep impact is in the vertical direction, which means more information about the GRF will be contained in the vertical vibration response. Next, we model the time history of the dynamic response of the floor structure as a single-degree-of-freedom system (SDOF) in which we assume a homogeneous structure (i.e., fixed mass, stiffness, and damping) and that the footstep excitations result from a constant gait (i.e., no irregular footsteps). We make this simplification to an SDOF system based on two primary assumptions. (1) For many residential buildings, individual floor bays typically consist of simply supported beams and continuous floor slabs. As a result, for gravity excitations (i.e., footsteps), the behavior of a simplified SDOF system closely resembles that of a multidegree-of-freedom system. (2) In this work, the relationship between vibration responses and footstep GRFs is modeled using physics-guided, data-driven approaches with little-to-no information available regarding the underlying structural properties, and any variations due to boundary conditions are absorbed into the model coefficients during model training. Based on this SDOF assumption, the formulation for the response is given by the following expression:

$$m\ddot{x}(t) + c\dot{x}(t) + kx(t) = F(t) \tag{1}$$

where $x(t)$ = displacement (deflection of the structure at time t); m = modal mass of the structure; c = structure damping; k = stiffness of the structure; and $F(t)$ = applied dynamic force (i.e., the footstep GRF).

For a linear, time-invariant system, the solution to Eq. (1) can be modeled using the well-known convolution integral formulation, as follows (Kelly 2012):

$$x(t) = \int_0^t h(t-\tau)F(\tau)d\tau \tag{2}$$

where $h(t)$ = impulse response function for the structure; and τ = time shift for the convolution integral.

As shown in Fig. 1(b) and discussed previously, we observe that the vibration signal is most correlated to the heelstrike transient from the footstep GRF. As a result, we model the footstep forcing function $F(t)$ as only the heelstrike transient portion of the overall GRF. The entire forcing function, $F(t)$, can then be represented as a normalized time-varying force multiplied by the peak amplitude of the heelstrike transient in the following way:

$$F(t) = F_0\widetilde{F(t)} \tag{3}$$

where F_0 = peak amplitude of the heelstrike transient portion of the footstep GRF; $\widetilde{F(t)}$ = normalized time-varying footstep ground reaction force; and t = time.

By substituting $F(t)$ from Eq. (3) into Eq. (2), we can see that the vibration response is proportional to F_0. In this work, we measure the velocity of the floor vibration ($\dot{x}(t)$) using geophone sensors (I/O Sensor Nederland bv 2006), which are low-cost mechanical vibration sensors. As such, we model the overall response based on the vertical velocity of the floor vibration (although a similar formulation could be done with acceleration if accelerometers were used in lieu of geophones). Geophone sensors are chosen over other vibration sensors (e.g., accelerometers) because they are low-cost and sensitive in the frequency bands typically excited by footstep-induced vibrations (Pan et al. 2017a). In this way, the overall footstep-induced vibration response is given by the following expression:

$$\dot{x}(t) = F_0 S(t) \tag{4}$$

where $S(t)$ = force-amplitude mapping function that depends on the dynamic properties of the structure (i.e., mass, stiffness, and damping) and the time-varying footstep GRF. From this expression, it follows that the peak value of the recorded vibration signal (in a given footstep-induced signal window) is proportional to the peak amplitude of the heelstrike transient. In this work, we utilize this relationship to develop a model for the mapping function between recorded vibration signal amplitudes and peak heelstrike transient response magnitudes (i.e., footstep forces). With this function, we estimate footstep GRFs and compare consecutive left-right pairs to determine gait balance symmetry.

However, the challenge with this approach is that the measured vibration amplitude is influenced not only by the magnitude of the footstep GRFs but also by the underlying structural behavior and sampling bias due to human walking tendencies. As previously discussed, the vibration signal is affected by spatial variations in the dynamic properties of the underlying structure (i.e., damping coefficient, stiffness, and mass), which we refer to as the *structural variation effect*. These changes affect $S(t)$ from Eq. (4) and result in a different relationship between the vibration signal amplitude and the footstep GRFs. As a result, a model trained in one region may not result in accurate force and balance estimations in an adjacent region if it has different dynamic properties. To overcome these varying properties, we note that variations in the dynamic properties of the structure result in changes to the frequency response spectrum of the structure (the frequency response function). In the "Structural Variation Effect Adaptation" section, we discuss how we leverage this insight to passively cluster footstep responses by structural region and develop mapping functions for each region independently.

In addition to the *structural variation effect* described previously, the vibration signal is influenced by vibration wave attenuation (Pan et al. 2014; Alajlouni et al. 2018). Attenuation is a well-known phenomenon with wave propagation through a given medium and results in the loss of vibration amplitude [$\dot{x}(t)$ from Eq. (4)] with increasing distance between the source (e.g., the footstep location) and the sensor (Stein and Wysession 2009). In structural vibrations, attenuation is best characterized by considering the dual-effects of structural damping (a.k.a., intrinsic attenuation) and geometric wave spreading (Stein and Wysession 2009). Fig. 2 shows an example of this attenuation effect (Fagert et al. 2017a). In this figure, the first footstep occurs close to the vibration sensor, and each subsequent footstep moves further from the sensor (increasing footstep-sensor distance). Note the decrease in the signal amplitude with increasing distance from the sensor location. As a result, it is not possible to directly compare measured vibration signal amplitudes and footstep GRFs at different locations. This requires a model that accounts for the footstep-sensor distance and the resulting attenuation of the vibration signal at this distance. The "Amplitude-Distance Attenuation" section explores this relationship in greater detail.

As discussed previously, the *gait sampling bias* on the GRF-vibration amplitude relationship describes the model bias resulting

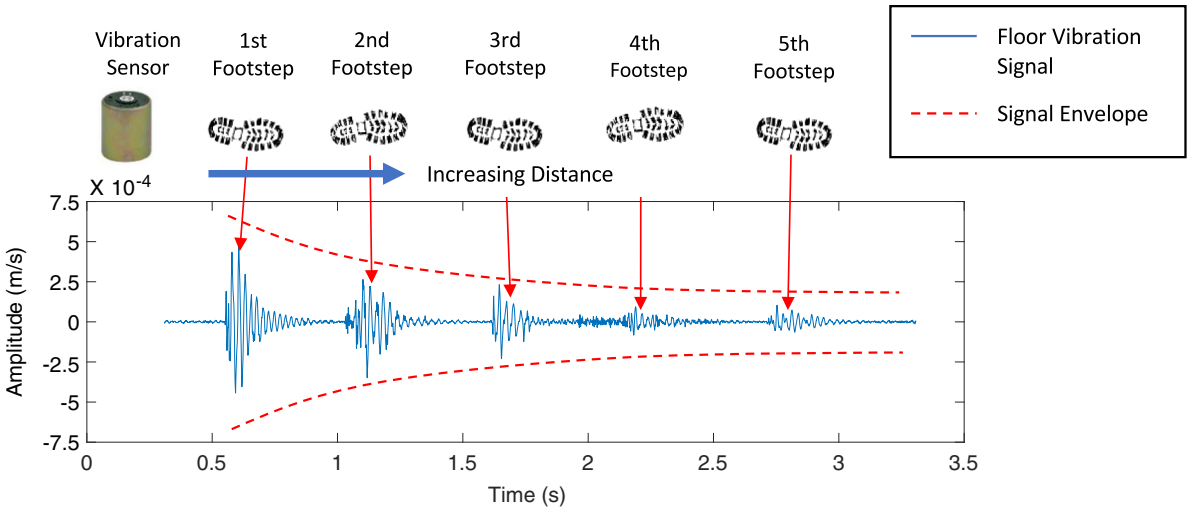

Fig. 2. Footstep-induced vibration responses for a series of consecutive footsteps. Note the decreasing vibration signal amplitude with increasing distance from the sensor.

J. Eng. Mech., 2021, 147(2): 04020151

from a narrow range of GRFs for a typical walker. Because of this, there is a concentration of training data near the mean of the GRF range, and extreme GRFs are not accurately estimated. In addition to this sampling bias, foot dominance causes variations in the footstep-floor relationship for each foot, causing errors in GRF estimation. This is caused by variations in walking between a person's dominant and nondominant foot. In a typical person's gait, the dominant foot is responsible for the propelling motion, while the nondominant foot tends to be primarily used for support (Peters 1988). As a result, the mapping function for the GRFs of the dominant foot is different from that of nondominant foot because the nature of the interaction with each foot and the floor structure varies. In the "Clustered Kernel-Based Learning" section, we show how our approach addresses both the *gait sampling bias* and the effect of foot dominance for robust footstep GRF and balance symmetry estimation.

Structure- and Gait Sampling-Adaptive Balance Symmetry Estimation

In our approach, we leverage the physical insights discussed in the "Physical Insight" section to estimate footstep GRFs and gait balance symmetry. Our gait balance symmetry estimation approach consists of three main modules: (1) a footstep detection and localization module, (2) a structure effect adaptation module, and (3) a clustered kernel-based learning module. Fig. 3 provides an overview of these modules.

The first module collects the raw vibration data from each sensor in the sensing area, extracts the portion of the signal that is induced by the footstep force, and finally determines the footstep location and corresponding footstep-sensor distance (for use in the next module). Next, we remove the distance-based attenuation influence on the signal by modeling distance-based amplitude attenuation and normalizing the vibration signal amplitude. To address the *structural variation effect*, we then use an unsupervised PCA-based clustering approach to characterize structural regions and independently model the footstep GRF-vibration signal amplitude relationship for each region. Then, in the clustered kernel-based learning module, we develop a new learning approach that first clusters consecutive steps as *dominant* and *nondominant* and then models the distribution of training data to develop a kernel-based robust regression and overcome the *gait sampling bias*. Through this learning approach, our method enables the estimation of footstep GRFs from footstep-induced vibration signal amplitudes. Finally, with the estimated footstep GRF, our system outputs the gait balance symmetry state using a metric known as the SI, which provides a percent ratio of left- and right-foot GRFs (Herzog et al. 1989; Sadeghi et al. 2000).

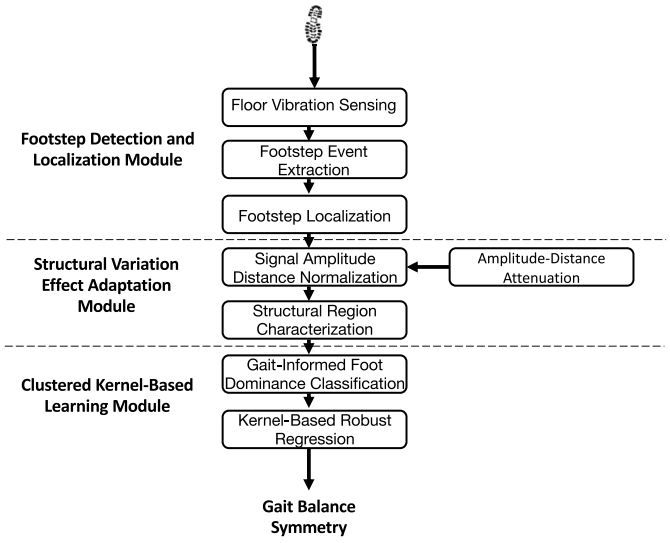

Fig. 3. Structure- and sampling-adaptive balance symmetry estimation approach.

Footstep Detection and Localization

In this section, the sensing system and approach for isolating footstep events from the raw vibration signal and estimating their location are presented. These detected, isolated, and localized footsteps are then used for the remaining modules of our approach.

Floor Vibration Sensing

Our balance symmetry estimation system collects footstep-induced structural vibration signals using floor-mounted geophone vibration sensors. Geophone sensors are mechanical vibration sensors that convert the velocity of the floor vibrations into an analog voltage signal. Because of the relatively small magnitude of footstep-induced vibrations and to increase signal resolution, we incorporate an operational amplifier (op-amp) into the sensing system. We select the gain of the amplifiers empirically by taking a series of footsteps near each sensor and selecting the gain which maximizes the amplitude of the footstep response while avoiding clipping of the signal. After amplification, our sensing system has an effective sensing range of up to 20 m (Mirshekari et al. 2018b; Pan et al. 2017b), which enables sparse sensor deployment and increases the gait balance monitoring range. For the collection of footstep-induced signals, a sampling frequency of 25.6 kHz is selected. We select this sampling frequency to (1) achieve sufficient time resolution for TDoA estimations (i.e., localization) and (2) ensure the fidelity of the frequency response for our structural region characterization (the typical footstep-induced response bandwidth is on the order of 0–250 Hz). An example of the sensing system used is shown in Fig. 6.

Footstep Event Extraction

To isolate footstep events from the overall vibration signal, our method framework consists of an anomaly detection algorithm that determines when the vibration signal exceeds an ambient noise level. Additionally, floor vibration signals often contain a mixture of impulsive events, such as objects falling and doors closing, as well as the footsteps of interest for this work. As a result, our event detection algorithm takes a two-stage approach in which we (1) detect impulsive events using a chi-squared hypothesis test and then (2) classify detected impulses as footsteps or nonfootsteps using a support vector machine (SVM) classifier (Lam et al. 2016; Mirshekari et al. 2018a, 2020).

The chi-square hypothesis is a common technique for anomaly detection and is based on comparing the variance in a given vibration signal window (e.g., 0.1 s) with that of the ambient noise conditions (i.e., when no impulses have occurred). Specifically, we compare the null hypothesis, H_0:$\sigma_w^2 \leq \sigma_n^2$, to the alternative hypothesis, H_1:$\sigma_w^2 > \sigma_n^2$, where σ_w^2 represents the sample variance of the current vibration signal window, and σ_n^2 represents the sample variance of the ambient noise conditions (Mirshekari et al. 2018b, 2020; Gingrich 1992; Baron 2013). We utilize this approach based on the observation that the ambient noise variance exhibits a chi-squared distribution, while impulsive excitations have a different distribution, which may be a different chi-squared distribution or another distribution altogether (e.g., Gaussian). As a result, impulsive excitations will result in a rejection of the null hypothesis (H_0). We empirically select the threshold for the hypothesis test based on

an initial calibration for the sensing area. When rejection of the null hypothesis occurs, our method marks the location of the anomaly in the time domain and sends this detected impulsive event for classification as a footstep or nonfootstep (Lam et al. 2016; Mirshekari et al. 2018a). Anomalies that are classified as footstep events are then extracted from the raw vibration signal and utilized in the remaining modules of our approach.

Footstep Localization

To localize the footstep event, we employ a TDoA-based multilateration algorithm based on our previous work that considers the propagation of the footstep-induced vibration wave through the floor structure medium. This algorithm contains two primary steps: (1) dispersion-invariant TDoA estimation (Mirshekari et al. 2016) and (2) footstep localization through locally adaptive multilateration (Mirshekari et al. 2018b). In the dispersion-invariant TDoA step, we overcome the tendency for the vibration waves of different frequencies to travel at different velocities through the structure (Lee and Oh 2016; Worden 2001) (known as dispersion) by decomposing the vibration signal in the time-frequency domain using a wavelet decomposition (Mirshekari et al. 2018b). This decomposition enables computation of TDoAs between each pair of sensors and for each frequency independently, thus mitigating the effects of dispersion. In the locally adaptive multilateration step, we use these TDoAs to estimate the footstep location without the need for calibration to find the wave propagation velocity. The detailed process for this multilateration approach is outlined in our previous work (Mirshekari et al. 2018b).

Once the footstep location has been determined, we next compute the footstep-sensor distance for each sensor in the sensing area. The footstep-sensor distance is defined as the Euclidean distance between the footstep location and each sensor location. For this computation, we assume that each sensor location is known and constant. We utilize these footstep-sensor distances in the next module of our algorithm to determine the expected vibration signal attenuation at each distance.

Structural Variation Effect Adaptation

Once a footstep event has been detected and isolated from the raw vibration signal, and its footstep-sensor distances are estimated, it is passed to the structural variation effect adaptation module of our method. In this module, we remove the effect of the distance-based attenuation on the vibration signal amplitude and address the *structural variation effect* challenge to our system. Our approach is developed using a two-stage framework in which we (1) develop a regression model to learn distance-based vibration signal attenuation and then (2) model structural regions with an unsupervised clustering algorithm.

The approach for each stage consists of the following steps.

- Stage 1. (1) We first extract the maximum vibration signal amplitude (absolute value) of the footstep vibration signal as a feature for footstep GRF estimation. (2) Next, the signal amplitude is normalized by a trained amplitude-distance attenuation curve to negate the distance-based signal attenuation.
- Stage 2. We model the frequency response of the footsteps and cluster them into structural regions based on a principal component projection and k-means clustering technique.

Amplitude-Distance Attenuation

To determine the attenuation rate for each sensor and the underlying structure, we develop an amplitude-distance function. By characterizing the attenuation rate for the instrumented structure, we use footstep-sensor distance information to normalize signals based on their anticipated attenuation. As previously discussed, the observed vibration signal amplitude is a function of the footstep ground reaction force and the signal attenuation. The signal attenuation is primarily influenced by two factors: (1) the intrinsic attenuation due to energy loss in the structural medium (i.e., damping) and (2) geometric wave spreading (Stein and Wysession 2009).

Intrinsic attenuation refers to the loss of vibration signal energy with increasing time (distance) traveled through a medium (i.e., the floor structure) (Stein and Wysession 2009). The rate of energy/amplitude loss for intrinsic attenuation is determined by the material properties of the floor structure. In the case of distance attenuation for footstep-induced floor vibrations, the effect of intrinsic attenuation is observed as a decrease in the vibration signal amplitude with an increasing distance between the footstep location and the sensor location (footstep-sensor distance) and can be estimated through the following expression:

$$A(d) = A_0 e^{\alpha d} \tag{5}$$

where $A(d)$ = vibration signal amplitude at a footstep-sensor distance d; A_0 = vibration signal amplitude at the impact location (where the footstep occurred); and α = material-dependent attenuation coefficient.

Geometric wave spreading describes the phenomena of a reduced vibration signal amplitude and energy as vibration waves expand outward from the location of the vibration-inducing impulse. This phenomenon is fundamentally caused by the conservation of energy; as the vibration wave covers additional surface area and volume (from spreading along the floor plane and throughout the floor depth), its total energy (and amplitude) remains constant but is distributed over the larger area/volume (Stein and Wysession 2009). With the vibration wave spreading at a constant rate, the amplitude attenuation due to spherical geometric wave spreading (for body waves) increases proportionally to the distance traveled (i.e., $A(d) = (A_0/d)$), while the circular/surface geometric wave spreading (for surface waves) increases proportionally to the square root of the distance traveled (i.e., $A(d) = (A_0/\sqrt{d})$) (Stein and Wysession 2009).

Total wave attenuation considers the combined effects of the intrinsic attenuation and geometric wave spreading as a concurrent reduction in amplitude with increasing footstep-sensor distance. From our prior work, we infer that the majority of the vibration response is a body/lamb wave (Mirshekari et al. 2018b; Pan et al. 2017a). However, for this work, we acknowledge that these body/lamb waves do not always represent the entire vibration response. Other aspects of the footstep-floor interaction (e.g., friction, horizontal components of the GRF, and so forth) may generate other waveforms, including surface waves. As such, in our treatment of the total wave attenuation, we include both of these potential waveforms by incorporating attenuation elements due to both surface and body wave geometric spreading. By including both terms, we are able to have more robustness to the in-place conditions as well as varying walking styles. Further, with this broad treatment of geometric wave spreading, we remove/reduce the need for prior information about the structure itself (which could be used for building a finite-element model for an analytical derivation of the total wave attenuation). Therefore, the total wave attenuation is estimated according to the following expression:

$$A(d) = \frac{A_0}{d\sqrt{d}} e^{\alpha d} + A_n \tag{6}$$

where A_n = vibration signal amplitude due to ambient vibration conditions; and unknown coefficients α and A_0 are as defined in Eq. (5).

To determine these coefficients, we model the distance-based attenuation using robust regression. Robust regression reduces the

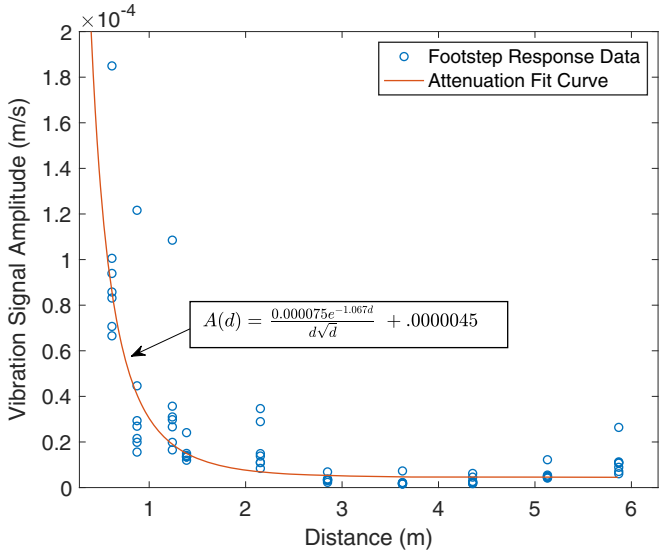

Fig. 4. Example of an amplitude-distance attenuation function. Using this function, our method normalizes vibrations signals to remove the effect of signal attenuation. Note that this function is trained independently for each sensor and building/structure, and the equation shown represents one example.

effects of outliers at small footstep-sensor distances by minimizing the L1 norm of the residuals (instead of the traditional L2 norm for the least-squares regression). Because of the high slope of the attenuation function in these small footstep-sensor distances, slight variations in the actual footstep location from the recorded ground truth location can result in large changes in amplitude (i.e., causes outliers). When training the amplitude-distance regression model, our system requires that footstep GRFs are consistent to avoid bias from overly large or small GRFs. To control this, training data is collected at a constant step frequency and with only one person. Fig. 4 shows an example of our amplitude-distance model, along with the coefficients from training for that particular sensor/structure combination. This process is repeated independently for each sensor in the sensing system, and the trained models are used for normalizing vibration signal amplitudes in the following sections.

Signal Amplitude-Distance Normalization

With each footstep that occurs in the sensing area, we evaluate the amplitude-distance function at its estimated footstep-sensor distance to obtain a normalization factor for that distance. Then, to obtain the normalized vibration signal amplitude, we divide the recorded vibration signal amplitude by the computed normalization factor. In this way, we are able to directly compare normalized amplitudes across a variety of footstep-senor distances, thereby enabling observation of changes in amplitude due to different footstep GRFs. We then utilize the normalized amplitude for estimating footstep GRFs.

Structural Region Characterization

To address the *structural variation effect* challenge, our system models spatial variations in the structure's frequency responses using an unsupervised clustering approach. This approach is based on the insight that the changes to the dynamic properties of the structure will result in varying the frequency content of the vibration response. In order to remove any bias due to the attenuation effect for footsteps in different locations, we normalize each coefficient of the frequency response by the peak amplitude of the collected signal. However, we note that the frequency responses alone may not accurately represent spatial variations in the structural behavior because (1) the signal is influenced by ambient noise, and (2) the vibration's response is dominated by the frequency components associated with the footstep excitation. Therefore, we project the frequency responses to a principal component space where we can decompose the signal into a representative basis that maximizes the data variance and reduces the influence of the system noise. Finally, we assign the decomposed response to a structural region-based cluster using k-means clustering.

In the *principal component projection* decomposition step of our structural region characterization, we transform the response to a set of principal components that maximize the variance of the feature distribution (Jolliffe 2002). In this portion of our approach, we define the feature space as the coefficients from the normalized frequency response of the footstep-induced vibration signals and create a matrix of footstep-induced responses. The principal component analysis (PCA) is an unsupervised linear transformation that is well-suited to linear, time-invariant systems (e.g., footstep induced floor vibrations). For our approach, PCA applied to footstep-induced vibration signals enables us to mitigate the influences of noise and dominance of the footstep-induced components of the frequency response by projecting the responses to a new set of bases where the variance is maximized.

We decompose the overall response by empirically selecting the first principal component and projecting the frequency response onto that principal component. We choose the first principal component based on the observation that this component has the largest coefficient values and therefore best represents the shared structural components of the footstep responses while also maximizing the data variance (enabling characterization of changes in these structural components).

Finally, with *structural region clustering*, we assign the projected frequency response feature vectors to a structural region cluster through unsupervised k-means clustering. K-means clustering is an unsupervised classification algorithm that develops clusters of data such that the Euclidean distance between individual points and the centroid of the cluster is minimized (MacQueen 1967). In this work, we take the number of clusters to represent the number of structural regions in the sensing area (which can be determined empirically by observing spatial changes in footstep-induced responses). For each footstep collected in the sensing area, we assign it to a cluster and utilize these clusters in our footstep force estimation step.

Clustered Kernel-Based Learning

In this module, we address the *gait sampling bias* challenge due to a narrow GRF range by creating a new learning approach, which combines gait-informed signal clustering (to separate dominant and nondominant footsteps) with a kernel-based robust regression analysis. Using the resulting regression model, our system estimates the footstep ground reaction forces and determines gait balance symmetry using the GRFs from consecutive footsteps.

Gait-Informed Foot Dominance Categorization

Once each footstep has been assigned to a structural region, we utilize human gait tendencies to separate each step into one of two distinct foot-based clusters. Our approach clusters each step based on the assumption that the person walking in the sensing area alternates between each foot for consecutive steps and that each walking trace is initiated with the same foot. Therefore, we place the first recorded step into one cluster and alternate assignments for each consecutive step.

Kernel-Based Robust Regression

With the structure-based clusters and alternating foot clusters, our method next models the footstep GRF-vibration amplitude mapping function using linear regression. For this regression, we independently model each cluster of structural regions and separate feet. Additionally, we note that the force-amplitude relationship discussed in the "Physical Insight" section will be influenced by the noise present in the system. For structural vibration sensing, this noise comes from two primary sources: ambient structural vibrations (e.g., machinery, HVAC systems, and so forth) and sensing system noise (e.g., sensor noise and circuit noise). Therefore, we formulate the GRF-vibration amplitude mapping function using the following expression:

$$\hat{F}_{0m} = \frac{\dot{x}_m + N_A}{S} + N_S \tag{7}$$

where $\hat{F}_{0m}$ = peak heelstrike GRF as estimated by sensor m; $\dot{x}_m$ = normalized vibration signal as measured by sensor m; S = mapping function factor at the time of maximum vibration signal amplitude; N_A = ambient vibration noise; and N_S = system noise. Note that due to the amplification of the geophone signals and normalization of vibration amplitudes for attenuation, a physical interpretation of the system and ambient noise is limited, but nonetheless, the coefficients N_A and N_S help to understand the relative effects of these types of noises for each structural region, foot, and sensing node (because each is trained independently).

We learn the mapping function using a robust regression-based approach. We utilize robust regression to reduce model bias to outliers that may occur from erroneous localization, vibration amplitude normalization, or ground truth footstep force measurements (Rousseeuw and Leroy 2005).

As discussed in the "Physical Insight" section, a narrow data range in footstep GRFs (i.e., most of GRFs are near the mean value) introduces a bias in these regression models. To overcome this *gait sampling bias* challenge, we introduce a weighting function to the robust regression that places higher weights on the extreme (high and low) GRFs and lower weight on the middle values (of which there are more instances). We adapt a weighted robust regression approach due to the insight that weighted regression is well suited for removing model sampling bias (i.e., the concentration of GRFs in our problem) (Little and Rubin 2019). We accomplish this robust weighted regression through an inverse kernel density-based weighting algorithm. The intuition behind this technique is that the probability density function (PDF) of the data has the highest value for the abundant central values of the GRF distribution and the lowest value for the extremes. Therefore, the inverse of the PDF will reflect the desired weighting values and reduce the bias due to the GRF distribution. In the case of footstep GRF data, the actual shape of the data distribution is unknown; as a result, we model the PDF using a kernel density estimator. We choose a kernel density estimator based on its flexibility with nonparametric distributions and the ability to estimate distributions with sparse data (Noh et al. 2012, 2015, ; Calfa et al. 2015; Racine 2008). In this way, we learn the PDF of the GRF data with the following expression (Noh et al. 2015):

$$f_x(x) = \frac{1}{nh}\sum_{i=1}^{n} K\left(\frac{x - x_i}{h}\right) \tag{8}$$

where $f_x(x)$ = PDF of the training ground truth footstep GRF data; n = number of training samples; K = kernel; x_i = training sample values; and h = smoothing parameter, which is optimized for the standard deviation and number of data points according to the process outlined by Bowman and Azzalini (1997). For our datasets, we assume that the variations in footstep forces are approximately Gaussian and select a Gaussian-based Kernel [given by $K(x) = (1/\sqrt{2\pi})e^{-\frac{1}{2}x^2}$], which enables a smooth approximation of the data distribution (Racine 2008). Fig. 5(b) shows an example of the estimated PDF for the footstep GRF data. Note the concentration near the center of the data distribution.

Using the weights obtained from the inverse PDF modeling described previously, our approach learns the regression coefficients (N_A, S, N_S) by minimizing the weighted L1 norm residual (WR_{L1}) across the entire training dataset according to the following cost function:

$$WR_{L1}(S, N_A, N_S, m, w_i) = \sum_{i=1}^{n} w_i \left| \left(F_{0mi} - \left(\frac{\dot{x}_{m,i} + N_A}{S} + N_S \right) \right) \right| \tag{9}$$

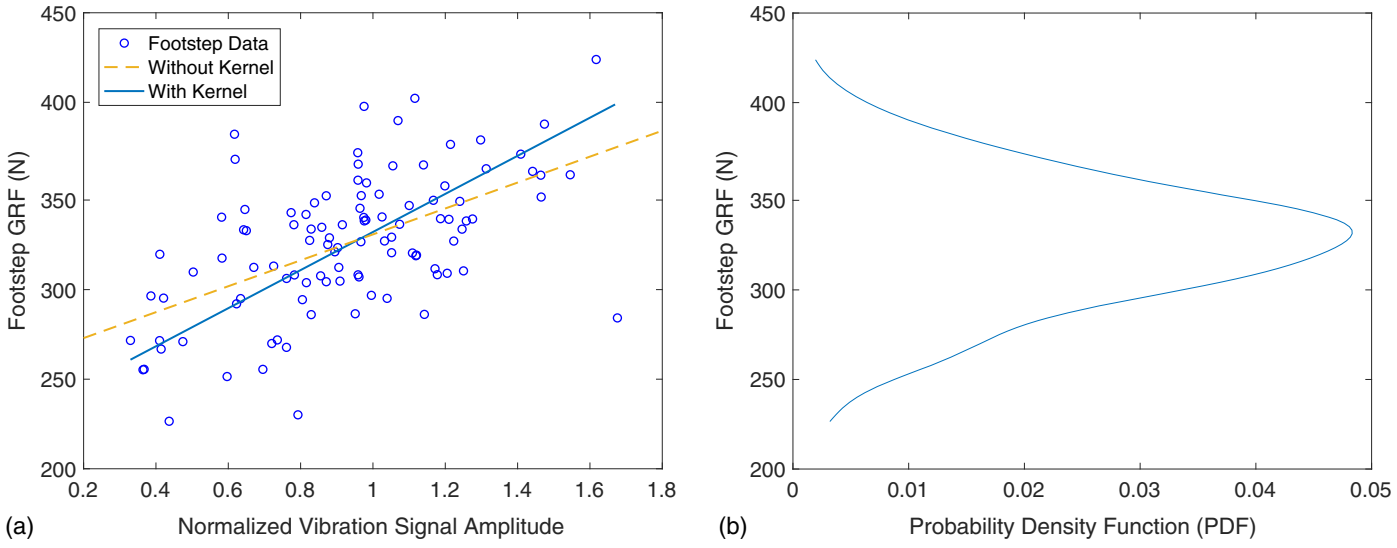

Fig. 5. (a) Example of the normalized amplitude-footstep GRF function using our weighted robust regression approach compared to the fit with an ordinary least squares regression (without kernel); and (b) associated GRF PDF obtained using a kernel density estimator. The inverse of this PDF is used to determine the regression weights.

where F_{0mi} = ground truth peak heelstrike GRF for step i; $\dot{x}_{m,i}$ = normalized vibration signal amplitude for step i as measured by sensor m; w_i = kernel density weights for each step; and S, N_A, N_S = coefficients to be learned through the robust regression. In our approach, we learn these coefficients independently for each sensor, structural region cluster, and foot cluster. Fig. 5(a) shows an example of the trained mapping function for one of the structure/foot clusters in which the orange line represents the trained mapping function values across the full vibration signal amplitude range.

Footstep GRF Estimation. Using the force mapping function, our method next estimates the footstep GRF and uses consecutive forces to estimate gait balance symmetry. To accomplish this, we combine the independent estimates from each sensor in the sensing area to obtain one overall force estimate. Our process for combining all of the sensor information is to take the average footstep GRF estimation across all sensors. However, we note that there are occasionally estimates from one or more sensors that are inconsistent with the rest. This may occur when the footstep location is too close to the sensor (where the amplitude normalization function has a very high slope). As a result, very small errors in the footstep location can result in very large changes to the normalization factor (and introduce high errors in the footstep GRF estimation). Therefore, to obtain our final footstep GRF estimation, we perform an outlier removal on the set of sensor estimates by removing those that are at least three scaled median absolute deviations from the median force estimate. This process allows us to remove the estimates from sensors in the sensing area that are much different from the rest and obtain an average force estimation that is not skewed by large errors. Once the outliers have been removed, our system outputs the footstep GRF as the average force estimate from the remaining sensors and uses this footstep force for balance estimation.

Gait Balance Symmetry Estimation. Once the footstep force has been estimated, our algorithm considers consecutive pairs of left- and right-foot footsteps to calculate gait balance. The SI is a common metric for assessing gait balance that compares the difference of two footstep forces to their average, with output as a percent balance symmetry using the following expression (Herzog et al. 1989):

$$S.I. = \frac{F_L - F_R}{0.5(F_L + F_R)} \times 100\% \tag{10}$$

where F_L and F_R = left- and right-foot footstep force estimates, respectively. Using the calculated SI, our system outputs a balance state as either *leaning left* (when $SI > 10\%$), *leaning right* (when $SI < -10\%$), or *balanced* (when $|SI| < 10\%$). We choose the threshold of 10% based on studies in the medical domain, which establishes this value as the threshold for the symmetric versus asymmetric gait (Hodt-Billington et al. 2012). Additionally, we note that the gait symmetry scenarios of most interest are those that are consistent across several footsteps (which removes false positives due to abrupt changes to footstep GRFs). As a result, we consider the average SI across the trace of footsteps (five consecutive left-right pairs of footsteps in this work) as the estimated SI of our system.

Gait Balance Symmetry Evaluation

To evaluate the performance of our system, we conducted real-world experiments with human walkers across different structures and with six experimental participants. In the following section, we first present our floor vibration sensing system and experimental setup. Next, we discuss the overall performance of our approach.

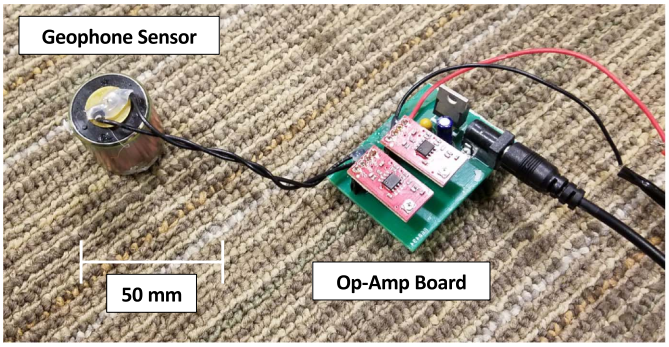

Fig. 6. Vibration sensing system.

Then, we explore the performance of our approach with respect to our research contributions. Finally, we evaluate the robustness of our approach by exploring its performance across different balance states, in different structures, and with different walking participants, respectively.

Experimental Setup

To evaluate the accuracy of our approach, we utilize a sensing system that consists of six geophone sensors. For this work, we select SM-24 geophones for our sensing system based on their low cost and small size for ease of retrofit in any structure (I/O Sensor Nederland bv 2006). The sensors are installed by adhering them directly to the floor surface using wax (which ensures coupling with the floor structure). As previously described, the amplification gain is set between 200 and 2,000X (depending on the structure) by selecting the gain that maximizes the footstep response amplitude while avoiding signal clipping. The sensing system used for this work is shown in Fig. 6.

The experimental evaluation was performed across three different structures, with six total participants and varying walking speeds and balance conditions. We chose the three locations as representative of common structural types: (1) the Baptist Homes Society, which is a wood-framed structure with a wood subfloor and carpet topping; (2) Porter Hall at Carnegie Mellon University, which is a noncarpeted concrete slab-on-grade structure; and (3) the Vincentian Home, a steel-framed structure with a carpeted concrete slab on the metal deck floor structure. Fig. 7 shows an example of the experiments conducted in each of the three structures. For each location, the number of structural regions was empirically specified as two based on the size of the experimental area, some prior knowledge of the underlying structure (e.g., locations of supports), and the preliminary experiments to observe footstep-induced signals in different areas.

Participants were asked to walk in a straight line at a speed controlled by a metronome for 12 consecutive steps and also at varying step frequencies and balance conditions. We define the 12 consecutive steps as a trace of footsteps, and each participant walked for a minimum of 5 traces. For our dataset, we remove the first and last steps of the trace to remove inconsistencies in walking when initiating and terminating movement. We selected step frequencies (speeds) of 1.25, 1.58, and 1.92 Hz based on normal human walking tendencies, which represent slow walking, medium/normal walking, and brisk/fast walking, in order to best represent the majority of walking tendencies in the general population (Tudor-Locke et al. 2011). To evaluate a full range of gait balance scenarios, three balance conditions were considered: balanced, leaning left, and leaning right. Fig. 8 shows the typical sensor layout

Fig. 7. Real-world experimental evaluation locations: (a) Baptist Homes (wood floor); (b) Carnegie Mellon University's Porter Hall (concrete slab-on-grade); and (c) Vincentian Homes (concrete slab on metal deck/steel framing).

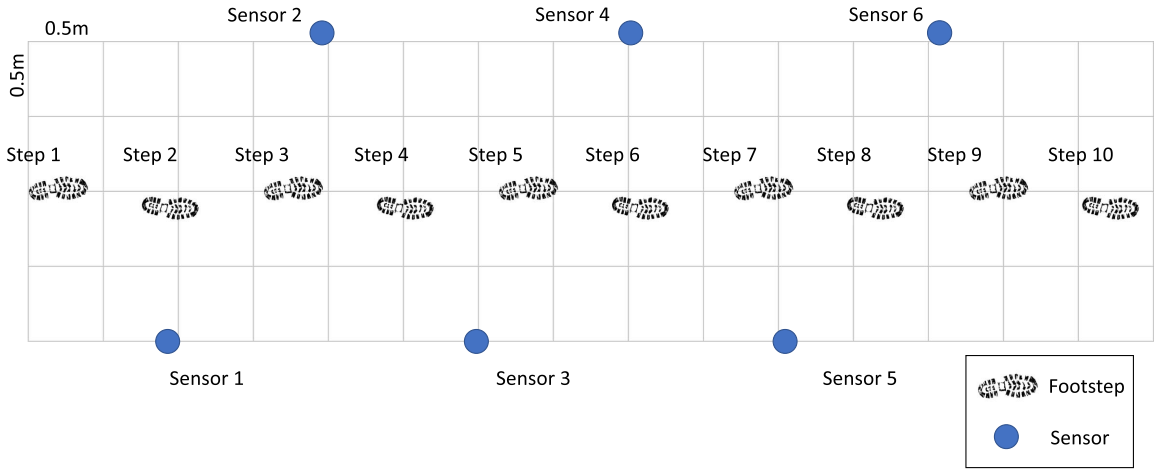

Fig. 8. Experimental setup. Typical sensor layout and footstep locations for walking experiments in the three structures.

and the ten remaining footstep locations used in the three experimental locations.

Ground truth footstep ground reaction forces were collected using pressure sensors mounted to the underside of the participant's shoe with a sampling rate of 1,000 Hz. This sample rate was selected to ensure that the initial heelstrike transient portion of the footstep GRF is able to be captured (as shown in Fig. 1). The synchronization with the geophone floor vibration sensors was done manually by asking participants to stomp three times with their heel prior to walking. The resulting impulses were then aligned in the time domain signals for the pressure sensors and geophone sensors. For this work, we utilized FlexiForce A401 pressure sensors (Boston), which are lightweight, flexible force sensors that can be placed on the bottom of the shoe without interfering with the ability to walk (Tekscan 2010). Pressure sensor data was collected separately for each foot using an Arduino Due and stored locally on a secure digital (SD) card to avoid the need for wireless communication and/or additional wires (which disrupt natural walking). Based on the discussion in the "Physical Insight" section, we concentrated the sensors on the heel of the shoe to ensure accurate measurement of the heelstrike transient. Across the experimental participants, walking speeds, and balance scenarios, we observed a peak heelstrike transient footstep ground reaction force range of approximately 130–450 N (30–100 lb).

Balance Symmetry Estimation Evaluation

In this section, we evaluate the overall accuracy of our approach for footstep ground reaction force (GRF) estimation and gait balance symmetry index estimation. To understand this overall performance, we consider the average accuracy of our system across all three experimental locations. We define this accuracy for each metric as follows:

$$\text{GRF Accuracy} = \frac{1}{n}\sum_{i=1}^{n} 100 - \left(\frac{|F_{0i} - \hat{F}_{0i}|}{F_{0i}} \times 100\right) \tag{11}$$

$$\text{SI Accuracy} = \frac{1}{k}\sum_{i=1}^{k} 100 - |SI_{\text{actual},i} - SI_{\text{pred},i}| \qquad (12)$$

where F_{0i} = actual peak heelstrike transient ground reaction force for step i; $\hat{F}_{0i}$ = estimated peak heelstrike transient GRF from our system; n = number of steps in the evaluation dataset; and k = number of consecutive pairs of left/right steps for the balance SI estimation. Note that SI is typically reported as a percent error, but we are reporting it as an accuracy for ease of interpretation.

For each evaluation metric, we compare our approach with a baseline approach. The baseline approach used for comparison is a naive approach, which learns a vibration amplitude–footstep GRF mapping function through an ordinary least squares regression without addressing the *structural variation effect* and *gait sampling bias* challenges of the system (i.e., no distance attenuation characterization, no structural region modeling, no foot bias removal, and no weighting to account for the small GRF range).

Our evaluation dataset consisted of a series of walking footsteps at varying speeds and balance scenarios across three different structures: the Vincentian Homes, Baptist Homes, and Porter Hall. For this overall performance evaluation, we analyzed 310 footsteps from the Vincentian Homes, 460 from the Baptist Homes, and 70 footsteps from Porter Hall. Each dataset was balanced with left- and right-foot footsteps. To analyze the overall performance, we independently trained and evaluated the three locations for GRF and SI estimation accuracy with a five-fold cross-validation. For this five-fold cross-validation, we randomly partitioned the datasets into five partitions and alternated training with four of the partitions and testing with the remaining partition. This process was repeated until all partitions had been tested.

For the overall evaluation dataset, we computed the average accuracy across each of the three structures by taking a weighted average of the performance in each structure (in which the weights are the number of steps in each structure). The resulting GRF and SI estimation accuracy is shown in Fig. 9. Our approach resulted in an average footstep GRF accuracy of 90.2% and an average balance SI estimation accuracy of 89.9%, which represents error reductions of 1.3X (86.9%) and 1.5X (84.7%), respectively, over the baseline approach.

From the overall results, we can observe that our approach is able to improve the baseline approach and achieve a high level of accuracy for force estimation. This increased performance of our system over the naive baseline approach is likely due to the fact that our approach is able to overcome the *structural variation effect* and *gait sampling bias* challenges described in the "Physical Insights" section. Because it does not address these effects, the baseline approach is not able to accurately model the relationship between footstep ground reaction forces and vibration signal amplitudes. This is further apparent in Fig. 10, where we observe that our approach accurately models the anticipated relationship (for every 1 N increase in the actual GRF, the estimated GRF increases by 1), while the baseline approach predicts approximately the same GRF regardless of the actual GRF. As a result, our approach achieves a higher accuracy for both the GRF estimation as well as balance SI estimation.

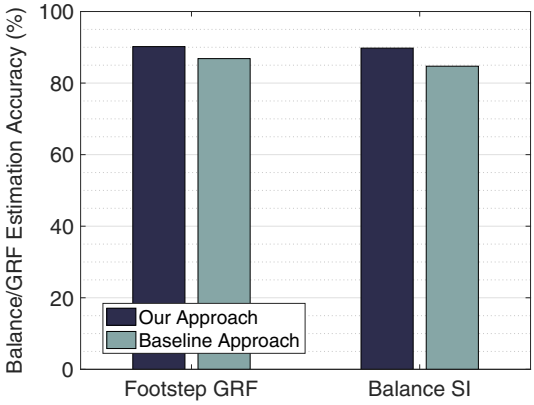

Fig. 9. Average performance of our approach for footstep ground reaction force and balance symmetry estimation across all three structures.

System Component Evaluation

In this section, we explore the performance of our approach with respect to each system component. First, we analyze the accuracy of our approach if each step of our method was removed (while keeping the others present). This enables us to observe the effect of each step of our method on the overall accuracy of our approach and determine the efficacy of our approach in addressing the primary research challenges of the *structural variation effect* and *gait sampling bias* on the GRF-vibration amplitude relationship.

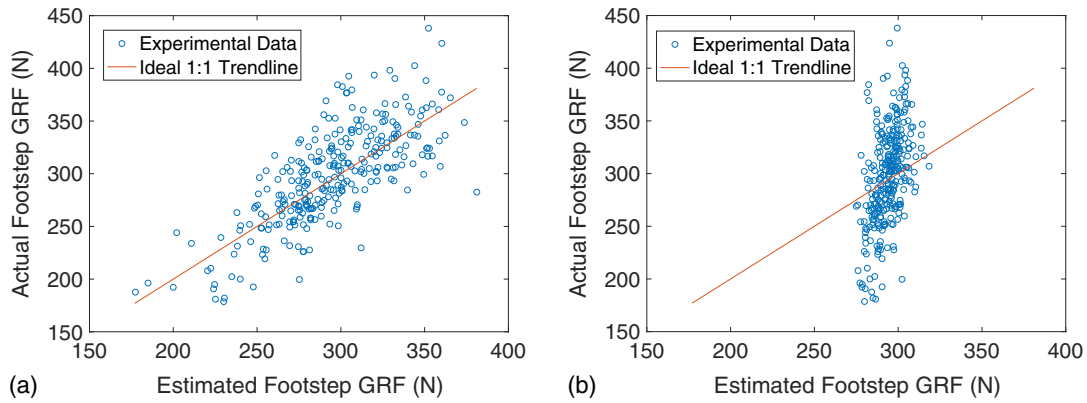

Fig. 10. Scatterplot of estimated forces versus actual forces for (a) our approach; and for the (b) baseline approach. Note that our approach follows the ideal 1:1 relationship between estimated and actual GRFs, while the baseline tends to predict a small range of GRFs despite an increasing or decreasing actual force. The line represents the ideal 1:1 relationship.

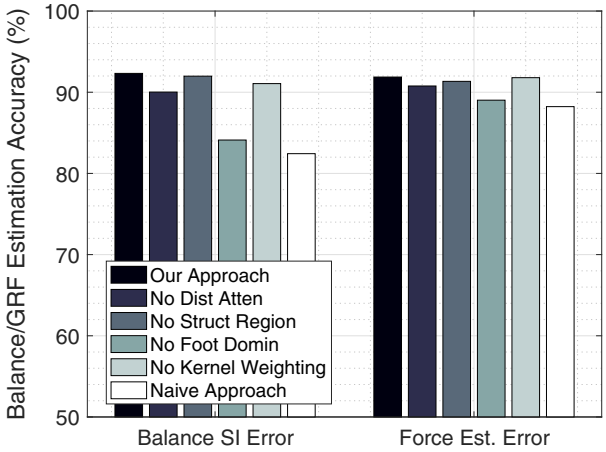

Fig. 11. Performance of our approach with respect to each step of the method.

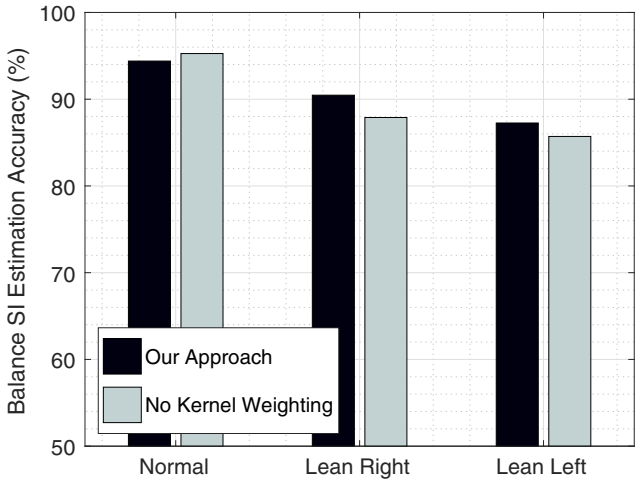

Fig. 12. Comparison of the performance between the overall approach and the no kernel-based robust regression for varying balance conditions.

Following this, we examine the sensitivity of our approach to localization errors.

Impact of Each Approach Component

We evaluate the improvement in footstep GRF and balance SI estimation for each step of our approach by comparing our overall approach with a series of alternative versions of our approach. Each alternative approach is a variation of our system in which one of the components from each module has been removed: one in which the effect of footstep-sensor distance attenuation is not considered, one in which variations in structural regions are not considered, one in which the effects of foot dominance are not considered, and one in which the kernel-based weighting is not performed on the regression fit. Finally, we present the naive baseline approach as a lower-bound comparison for each approach. For this evaluation, we consider the data from one participant in our Vincentian Homes experimental location. This enables a more detailed analysis of the impact of each component of our system.

The results of this comparison are shown in Fig. 11. As can be seen in the figure, our approach outperforms each of the alternative approaches for both footstep GRF estimation and trace-level balance SI estimation, which indicates that each step in our approach is necessary to capture the most accurate floor vibration-footstep GRF mapping function. Specifically, our method achieves an average GRF estimation accuracy of 91.9% compared to the alternative approaches, which show accuracies of 90.8% (no distance attenuation), 91.3% (no structural region clustering), 89.0% (no foot dominance), 91.8% (no kernel-based robust regression), and 88.2% (naive approach). For a balance SI, our approach results in an average accuracy of 92.3% compared to 90.0% (no distance attenuation), 92.0% (no structural region clustering), 84.1% (no foot dominance), 91.1% (no kernel-based robust regression), and 82.4% (naive approach). Further, we note that the foot dominance appears to have the most significant effect on the accuracy of our approach with respect to the naive baseline. This observation not only indicates that isolating this effect allows us to better capture gait balance information but also supports findings in the medical domain regarding the variation in footstep-floor interactions between dominant and nondominant feet.

To fully compare the performance of the overall approach with the no kernel approach, it is also necessary to consider how each performed with regard to varying balance conditions. The primary benefit of the kernel weighting is that it improves the balance symmetry estimation in unbalanced conditions (which are most critical with respect to assessing overall gait health). To evaluate this, we considered the performance of our overall approach compared to one that does not include the kernel-based robust regression in the varying balance conditions. Fig. 12 shows these results. From these figures, we can observe that the overall approach outperforms the no kernel approach for balance SI estimation in each case in which an imbalance is present (90.5% versus 87.9% for lean right and 87.3% versus 85.7% for lean left), while performing worse in the normal case (94.4% versus 95.3%). This better performance for no kernel in the normal scenarios is to be expected because there is more training data for normal scenarios.

To further evaluate the performance of the structural region clustering approach presented in this work, we conducted an additional evaluation across varying degrees of difference in structural behavior. In the comparison shown in Fig. 11, we considered the difference between our approach and an alternative *no structural region* approach. However, at the scale of the experiments conducted (approximately 2×8 m), the change in the underlying structure was rather minor. This is likely due to the fact that adjacent areas of a floor typically have similar underlying support conditions. As such, significant changes in the GRF-vibration amplitude relationship likely occur over larger areas than the ones tested (which were constrained due to space limitations in the experimental locations). Our prior work conducted in the hallway and adjacent rooms of a townhouse showed that different regions in the structure could generate vibration responses with a difference in peak amplitude of as large as 2X greater (Pan et al. 2014).

To illustrate how our PCA-based structural region clustering performs when there are more significant changes in the structural behavior, we simulated changes to the vibration signal amplitude at various magnitudes. Based on our observation that the vibration amplitude can vary as much as 2X, we modified the vibration amplitude for Region 2 in the Vincentian location (the same as used in the preceding comparison) to simulate how our approach and the alternative approach would perform when the degree of structural difference is 1.3X, 1.6X, and 2.0X. We chose to modify the Region 2 amplitude based on the fact that fewer footstep locations were clustered into this region (meaning less available training data for our approach and more difficulty in accurately estimating steps in this region). In this case, if the variations in the GRF-vibration amplitude relationship are not accounted for, those footstep GRFs will not be accurately estimated.

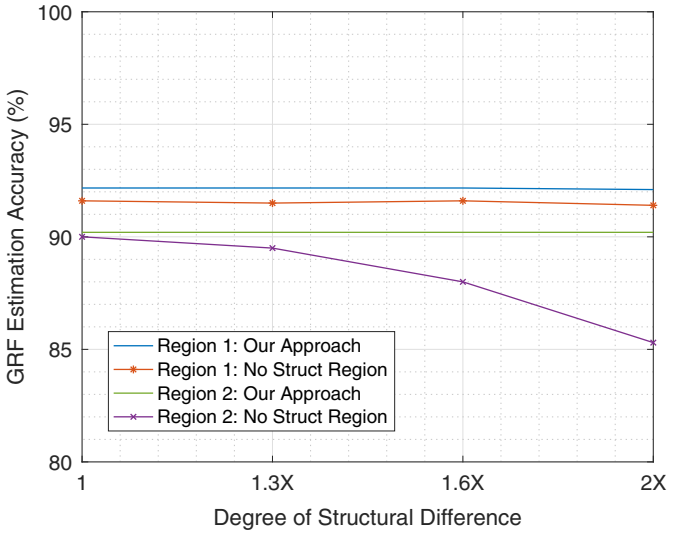

Fig. 13. Comparison of the performance between the overall approach and the no structural region clustering for varying degrees of structural difference.

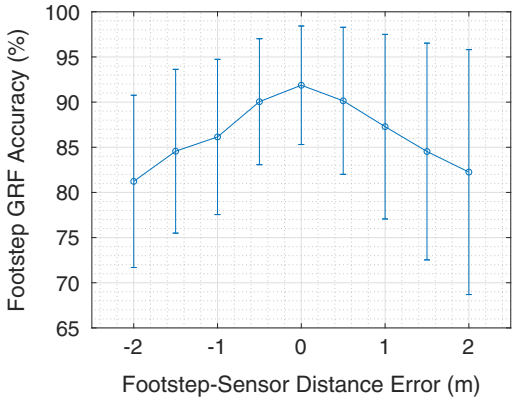

Fig. 14. Force estimation accuracy with varying footstep-distance error. The average error is given by the markers at each distance error increment, with one standard deviation of accuracy provided by the vertical lines.

The results of this comparison are given in Fig. 13. From this figure, we can observe that our approach has a constant accuracy for both Region 1 steps (approximately 92.2%) and Region 2 steps (approximately 90.2%). In contrast, the alternative approach, which does not account for structural regions, has decreasing accuracy in Region 2 with increases in the degree of structural difference (90.0% to 85.3%) but an approximately constant performance for Region 1 (approximately 91.6%). The constant performance for Region 1 in the alternative approach is likely due to the imbalance in training data for that region (approximately 80:20 split between Region 1 and Region 2), so the alternative approach accurately characterizes the GRF-vibration amplitude relationship for Region 1 but does not do so for Region 2.

Sensitivity to Localization Error

To understand the sensitivity of our approach to localization error, we consider the accuracy of our method at varying levels of error in estimating the footstep location and corresponding footstep-sensor distance. To simulate the localization error, we train our model using known footstep locations; then, for the test footsteps, we introduce localization error into the amplitude normalization module. We introduce this error as an increase or decrease in the footstep-sensor distance and vary the amount between −2.5 and +2.5 m at 0.5-m increments. For this evaluation, we again consider the Vincentian Homes experimental data for one participant and compute the average GRF estimation accuracy across a five-fold cross-validation.

The resulting footstep force estimation accuracy is shown in Fig. 14. In this figure, the average accuracy across all five folds for the test footsteps at each distance error increment is shown with markers, with one standard deviation of accuracy given by the vertical lines. In this case, the standard deviation given is computed across the entire test dataset for that level of distance error. Based on our prior work, our localization approach achieves an average error of 0.34 m (Mirshekari et al. 2018b). With this level of distance error, the resulting GRF accuracy is approximately 91.1%, which would result in less than a 2% additional GRF estimation error from the ideal case (0 m error). Further, with as much as a 0.5-m distance error, our approach has an average accuracy of 90.0%, which is still an improvement over the naive baseline approach, with no effect from localization (11.8% error). Lastly, we note that the force estimation accuracy is lower when the distance error is negative (as compared to a similar positive error). This likely is a result of the slope of the amplitude-distance function described in the "Amplitude-Distance Attenuation" section. As the footstep-sensor distance is increasingly smaller, the slope of the amplitude-distance normalization curve is increasingly steep, so introducing additional error in this distance range will result in large changes to the normalization factor and, consequently, introduce additional GRF estimation errors.

Balance State Robustness Evaluation

To evaluate the robustness of our approach to different balance states and different step frequencies (walking speeds), we take a detailed look at our Vincentian Homes location for one person's data. We focus on a singular walker and one location for this evaluation in order to best isolate the influence of varying balance states and step frequencies. We asked our experimental participant to walk at the same three different step frequencies as before: 1.25, 1.58, and 1.92 Hz. During the experiments, the walking speed was controlled by a metronome, and the participant was asked to take 1 step at each tone of the metronome. For the three balance scenarios, we considered balanced in which the participant was asked to walk normally, leaning right in which the participant was asked to place more weight on the right side of their body while walking and leaning left in which the participant was asked to place more weight on the left side of their body while walking. For the varying balance scenarios, the shoe-mounted pressure sensors were used for ground truth in determining if there was an imbalance toward one side or another. Due to the variability in the participants mimicking an imbalance condition, there was a range of SIs from these experiments that varied from slightly imbalanced to significantly imbalanced. From the ground truth information, this balance SI range was as follows: −1% to 50% for lean left and −22% to 7% for lean right. Because this also represents potential real-world balance conditions, we did not modify the datasets in any way. Further, because we consider trace-level balance SI for our final prediction (average across 5 pairs of steps as described in the previous "Gait Balance Symmetry Estimation" section), in each trace, the average SI correctly corresponds to the command given (lean right or lean left). For this robustness evaluation, we take a detailed look at the results from our Vincentian Homes location, and our evaluation

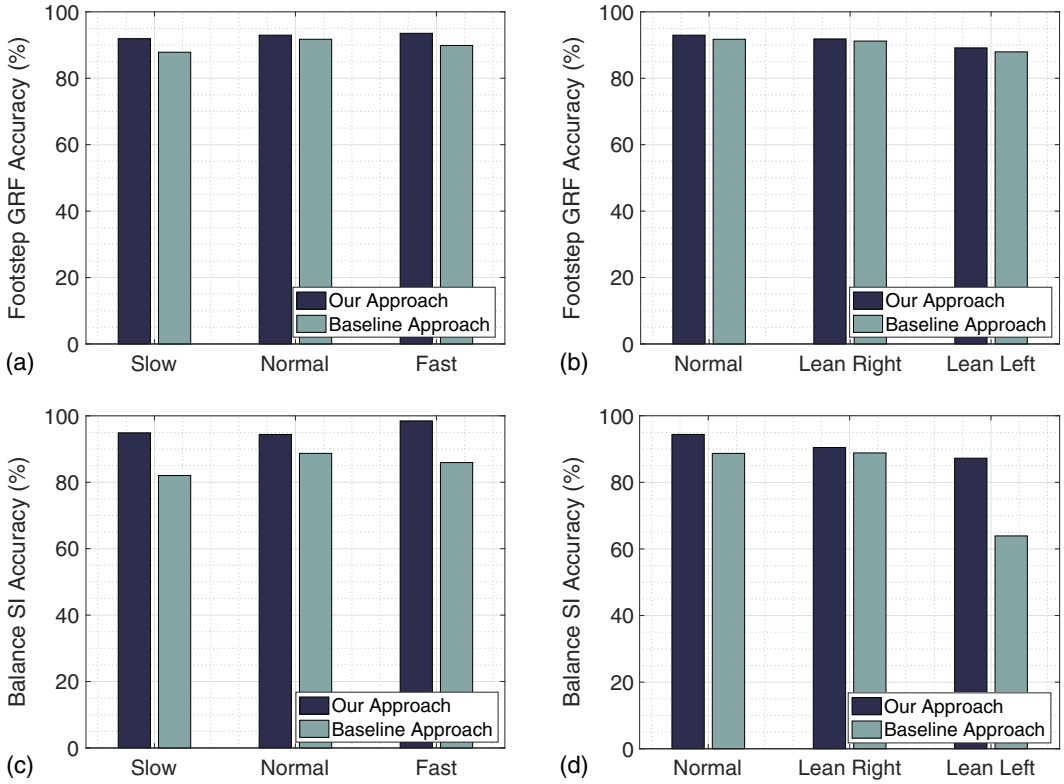

Fig. 15. Force GRF estimation and balance symmetry index estimation accuracy for Vincentian Homes across different walking speeds and balance conditions. Note the improvement over the baseline approaches for the lean right and lean left conditions, which are particularly useful for condition diagnosis.

assumes that the training data consists of a mixture of data from each speed and balance scenario, while the test data is independently evaluated for each scenario. Similar to previous evaluations, we performed a 5-fold cross-validation on the dataset to ensure that each sample had been both used for training as well as testing.

In our balance state robustness evaluation, our method realized an average force estimation accuracy of 91.9%, 93.0%, 93.5%, 91.8%, and 89.1% for the slow, normal, fast, leaning right, and leaning left conditions, respectively. These represent an average error improvement of 1.3X from the baseline approach. For balance SI estimation, our method results in the average SI estimation accuracy of 94.9%, 94.4%, 98.5%, 90.5%, and 87.3%, for the slow, normal, fast, leaning right, and leaning left conditions, respectively, which corresponds to an average error reduction of 3.7X from the baseline approach. A summary of the results from the varying balance state and step frequency conditions is shown in Fig. 15.

From these results, we can clearly observe that our method consistently outperforms the naive baseline approach for both the balance SI and for footstep GRF estimation across each of the scenarios considered. Further, we note that our approach has a similar performance across each of the speed and balance scenarios with the exception of leaning left. In the leaning left scenario, both our approach and the baseline approach have lower accuracy for the balance SI and GRF estimation, but our method is still able to achieve as much as a 2.8X error improvement from the baseline approach. The lower accuracy for this scenario is likely a result of the participant artificially simulating an unbalanced scenario while walking. The participant considered for this evaluation indicated that their dominant foot is their right foot, which means that placing additional weight and favoring the left side while walking likely resulted in a change in the walking style of the participant. Additionally, because this new walking style is not natural to the participant, we observed a larger range of ground truth footstep GRFs in this scenario. In contrast, for real-world applications of our system, persons with gait asymmetries will likely have gradual changes in their balance state and/or be consistently favoring one side or the other while walking. In these scenarios, there will likely be much less variance in footstep GRFs from one step to the next, and we expect that our approach will better capture the gait balance and footstep GRFs. Through our collaboration with Vincentian Homes and Baptist Homes, our future work will aim to include walking data from senior residents with known gait asymmetries so that we can improve the robustness of our method to these conditions.

Robustness to Different Structures

To evaluate the robustness of our approach to varying structural conditions, we make a detailed comparison of its performance across our three experimental locations in this section. As discussed previously, these structures represent a variety of structural supports (Vincentian—steel, Baptist—wood, and Porter—concrete); by evaluating across each of these structure types, we ensure our approach is robust to varying structural conditions. In each structure, we compare the results of our approach with those of the naive baseline approach discussed in the "Gait Balance Symmetry Estimation Evaluation" section for the same structure.

For our Vincentian Homes location, our approach achieves an average footstep GRF accuracy of 91.9%, which represents a 1.5X improvement over the baseline approach accuracy (88.2%). When considering trace-level balance SI estimation, our method results in an SI average accuracy of 92.3%, while the baseline approach has

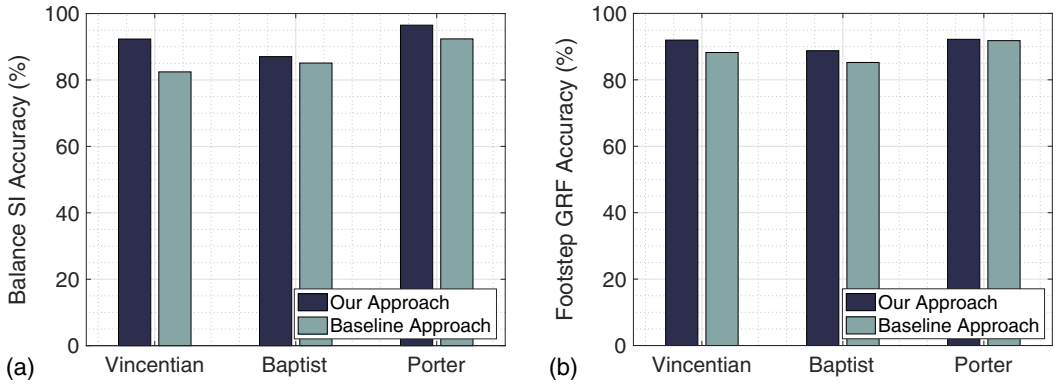

Fig. 16. Balance SI and footstep GRF estimation accuracy for our approach compared to the naive baseline approach in different structures.

an average accuracy of 82.4%, representing a 2.3X reduction in error from the baseline approach. In Baptist Homes, our approach achieved an average footstep GRF accuracy of 88.7%, which represents a 1.3X error improvement over the baseline approach (85.2%). For balance SI estimation, our approach achieves an accuracy of 87.2% (1.2X baseline improvement). Lastly, in Porter Hall, our approach achieved an average footstep GRF accuracy of 92.4%, which represents a 1.1X error improvement over the baseline approach (92.08%). Then, for balance SI estimation accuracy, our approach achieves an average accuracy of 96.5% (2.2X baseline improvement). Figs. 16(a and b) show the performance of our approach versus the naive baseline approach for the three experimental structures.

When considering the results from each of the experimental locations, we note that the force estimation accuracy is similar for each location and that each location achieves a level of SI estimation accuracy that indicates its effectiveness for gait balance assessment. However, we do note that the force estimation and balance SI accuracy are both slightly higher for Porter Hall as compared to the other two locations. The reason for this likely has to do with the nature of the underlying structures at each location. At Porter Hall, the underlying structure is a concrete slab-on-grade, while at Baptist Homes, the floor is constructed of wood framing, and Vincentian Homes is constructed of steel framing and concrete floor slabs. With a concrete slab-on-grade, the underlying structure is more homogeneous and less spatially-varying (as compared to steel and wood). As a result, the structural behavior is more uniform, which results in more consistency for the footstep GRF-vibration signal amplitude relationship and, consequently, higher estimation accuracy.

Robustness to Different Walkers

To evaluate the robustness to different people, an additional set of experiments was conducted at the Porter Hall experimental location. At this location, five participants of different ages, genders, and heights/weights were asked to walk in the sensing area for 10 steps in succession. Due to the corruption of the ground truth data, the sixth experimental participant was excluded from this evaluation. Participant ages ranged from 20 to 60, heights ranged from 165 to 185 cm, and weights ranged from 52 to 116 kg. Across the 5 participants, a total of 350 footsteps were recorded. Ground truth forces were again collected using a shoe-mounted pressure sensor, and the same shoe was worn by each participant (to remove possible bias from footwear), which was a leather boot with a hard leather sole. We conducted this experimental evaluation in conjunction with our approved IRB (Noh et al., "Structures as sensors: Elder activity level monitoring through structural vibrations," STUDY2015-00000125, unpublished report, submitted to Carnegie Mellon Univ., 2015).

From our preliminary experiments, we observed that the footstep ground reaction forces are influenced by the subject's weight. Gait parameters, such as speed and stride length, have been shown to be influenced by body weight (Samson et al. 2001); when these and other gait parameters change, it affects the interaction of the foot and the floor structure, which, in turn, influences the footstep ground reaction force-vibration amplitude relationship. To accommodate this weight effect, we assigned the participants into two distinct weight groups: 52–70 kg and 86–116 kg. For each group, we pooled the participants' footstep data into one dataset and evaluated that group's accuracy with a five-fold cross-validation (as described previously). Therefore, the two evaluation scenarios that were investigated with this experimental data are (1) a combination of Persons 1, 4, and 5 (the lower weight group) and (2) a combination of Persons 2 and 3 (the higher weight group).

For Scenario 1, our method achieves an average footstep GRF estimation accuracy of 91.3%, 70.0%, and 87.1% for Persons 1, 4, and 5, respectively. For Scenario 2, our method achieves a 93.0% and 71.5% accuracy for Persons 2 and 3, respectively. Fig. 17 shows the accuracy for estimating each participant's footstep forces, with each bar representing the average accuracy for each foot of the participant. For the balance SI estimation, our approach achieves a high accuracy for Persons 1, 2, 4, and 5 (93.8%, 93.7%, 88.9%, and 93.6%) and an accuracy of 69.6% for Person 3. Fig. 18 shows an overview of our system's balance SI estimation accuracy for different people. These results indicate that our method is appropriate for assessing gait balance and can do so with high accuracy across different persons.

In the robustness to different persons evaluation, we can make several significant observations about variations in walking style as well as health status. The first observation is with respect to Person 3. As noted previously, our method resulted in large estimation errors for right foot forces (and subsequently balance SI) for this particular participant. After exploring these results, we learned that this particular participant recently underwent knee replacement surgery for their right knee and indicated that this knee was still healing. As a result, the manner of walking from one step to the next is highly variable as the participant is adjusting to their new walking style. In our experimental results, we observe this phenomenon; while the majority of estimations are accurate (less than 10% estimation error), there are several where the ground truth force is very low (less than 1/3 of the normal range), but our estimation is high (above typical estimated values). This observation is likely the direct result of a change in the foot contact angle or contact location (heel versus midfoot versus toe) as the participant is coping with a healing knee.

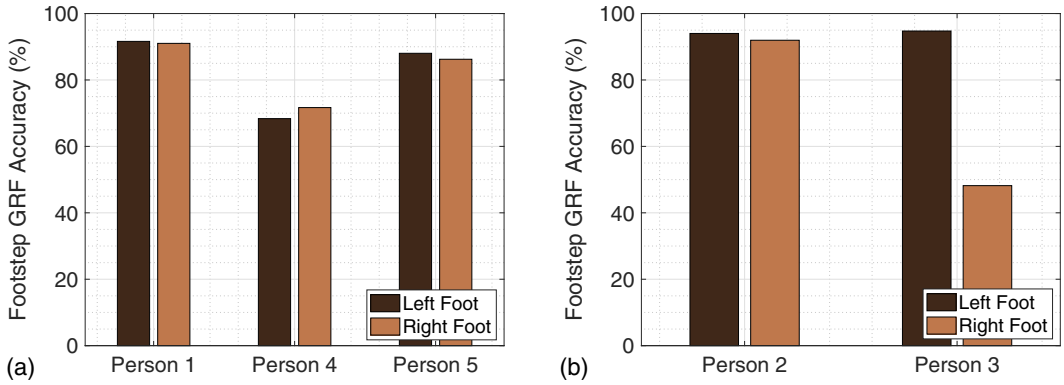

Fig. 17. Porter Hall accuracy for different walkers: (a) three of the five participants with a similar weight (52–70 kg) were evaluated together; and (b) the remaining two participants with similar weight (86–116 kg) were evaluated together. Note that the low accuracy of the right foot of Person 3 may be due to a recent knee replacement surgery for that person.

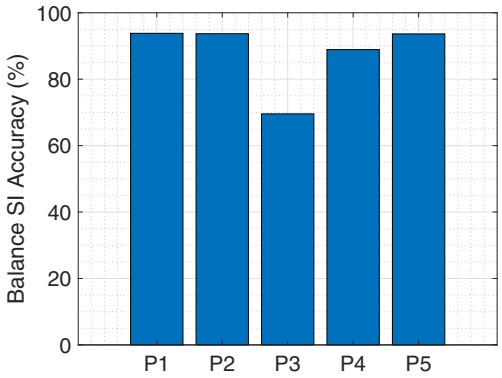

Fig. 18. Balance SI estimation accuracy for each experimental participant. Our system achieves high accuracy for Persons 1, 2, 4, and 5, indicating that it is robust to different walkers. Person 3 recently underwent knee surgery, which could influence walking variability.

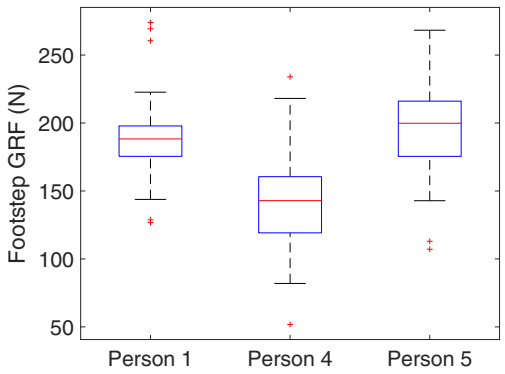

Fig. 19. Comparison of footstep GRFs for Participant group 1. Note the lower distribution of GRFs for Person 4, which indicates that this person does not place as much force on their heel during the initial contact as Persons 1 and 5.

Because our approach is still able to capture footstep force information in these scenarios, it shows promise for the ability to diagnose changes due to injury or surgery, but further work is necessary for understanding variation due to the footstep initial contact location. In our future work, we plan to characterize these initial impact locations (i.e., back heel, mid heel, and toe) and identify when these impact locations vary, which will provide additional gait health and balance symmetry information.

For the force estimation of Person 4, we note that our approach consistently overestimates the ground truth forces. Additionally, we note that the majority of the ground truth forces are lower than those of Persons 1 and 5 from the same group. Fig. 19 shows this observation using a boxplot of the measured heelstrike GRFs. In this figure, the box represents the interquartile range (from the 25th to 75th percentile of the data distribution), the whiskers represent the approximate data distribution limits (1.5x the interquartile range), and the crosses represent statistical outliers. From this figure, we observe that the heel impact GRFs for Persons 1 and 5 are higher on average than those for Person 4. This implies that Person 4 may be walking differently than the others by impacting further toward the front of their foot. As a result, the ground truth force collected by the back-most sensors will be low, while the vibration signal measured by our sensors will remain higher. We plan to explore these interfoot pressure distribution changes in our future work so that our system can better address individual variations in interfoot contact location.

Discussion and Future Work

In this paper, an approach for estimating footstep ground reaction forces and gait balance symmetry using footstep-induced vibration sensing is presented. The results of a real-world experimental evaluation with six total walking participants and three experimental locations indicate that this approach is promising for nonclinical assessment of occupant gait health parameters. In this section, we explore the relevant assumptions and limitations of this work and discuss future research directions that aim to address those limitations.

Multiple Walkers

In this work, footstep ground reaction forces and balance symmetry were evaluated through a series of controlled experiments with one walker in the sensing area at a time. However, in real-world scenarios, it is likely that multiple persons are walking concurrently in any given area (either together or passing by one another). As such, vibration responses from footsteps are often overlapping and mixed, making it difficult to uniquely estimate the GRFs and

balance symmetry for each person independently. To address this limitation, we have prior work that shows that we can uniquely identify individuals with up to 96% accuracy (Pan et al. 2015, 2017c), as well as preliminary work with *multiple walker* scenarios (Fagert et al. 2019c; Shi et al. 2019). In our future work, we plan to combine these works on identification and the GRF/balance estimation approach described in this paper to enable gait health assessment in a variety of indoor scenarios.

System Deployment and Scalability

An important discussion for any sensing system involves its deployment/maintenance costs and scalability in real-world scenarios. As discussed in the "Related Work" section, the system used in this work has the benefits of being passive and sparse while also reducing concerns related to privacy. For building-scale deployments, these benefits are especially prominent. Regarding deployment/maintenance costs, we estimate that at a large scale, the sensing nodes can be purchased at a relatively low cost (Pan et al. 2017a). Further, they are easily installed on the floor structure (they only require coupling with the floor through a bonding agent such as wax) both in new construction and retrofit scenarios. In consideration of scalability, we have also developed a wireless version of the sensing system to reduce installation and maintenance costs (i.e., cable maintenance). The wireless system communicates over WiFi for the purpose of data transmission and synchronization.

To enable the GRF/balance symmetry estimation described in this work, as few as three sensors are needed in the walking area [primarily for localization purposes (Mirshekari et al. 2018b)], and we have observed a sensing range of up to 20 m by optimizing the variable gain of the amplifiers (Pan et al. 2014, 2017b).

In addition to the preceding discussion, the topic of scalability within a building is an important consideration. In this work, one of the primary contributions is the ability to adapt to spatially-varying structural properties through a PCA-based clustering approach. At the scale of the experiments conducted for this work, the number of structure regions was empirically chosen to be two. For our future work, we intend to explore how this concept can be expanded to automatically characterize the number of structural regions based on changes in vibration signals and/or expanded by using prior information about the underlying structure (e.g., locations of columns, primary beams/girders, and so forth).

Additional Gait Factors

One of the primary assumptions for the GRF/balance symmetry approach outlined in this work is that the current system assumes that initial contact is made with the heel (i.e., the heelstrike transient relationship). However, as discussed in the "Robustness to Different Walkers" section of the experimental evaluation, one limitation of this assumption is when persons have abnormal gaits and make initial contact with a different part of their foot (e.g., midfoot or toe). In these scenarios, the system would predict a larger GRF for the heelstrike transient when, in fact, it was quite low and/or nonexistent. As such, in our future work, we plan to investigate in-foot pressure distribution through decomposing the vibration response and mapping the components of the response to individual portions of the footstep pressure distribution. Some of our preliminary work in this area shows promise for distinguishing between initial contact with the heel and with the toe (Dong et al. 2020). This will enable us to expand our system into a comprehensive gait analysis platform where additional parameters, such as in-foot pressure distribution, the center of pressure, and movement of the extrapolated center of mass, can be evaluated in real-time and in a variety of indoor, nonclinical environments.

Beyond variations in walking style, in-foot pressure distribution and the GRF-vibration amplitude relationship may be affected by the shoe type. In this work, the effect of different shoes was controlled by having each participant wear the same shoe (a hard-soled boot). However, in real-world scenarios, people may wear soft-soled shoes, be barefoot, and/or wear shoes with heels. In these situations, both the nature of the foot impact is affected, as well as the contact location on the foot (especially in the case of high-heeled shoes). In our future work, we will explore the effects of shoe shape and sole hardness on the footstep GRFs, the mapping function between them, and the measured floor vibration signals.

Lastly, in this work, we leverage the physical insight that dominant and nondominant feet serve different functions during gait and develop independent GRF-vibration amplitude models for each foot. The process for developing these independent models in this work assumes that each step is with alternating feet, and experiments were controlled to instruct each walker to start with the same foot for each walking trace. As such, this work does not attempt to characterize which foot is dominant and which is not. However, based on the findings (in which foot dominance plays a significant role in the accuracy of the overall approach), there is reason to believe that the sensing system used in this work could also be used to characterize which foot is the dominant foot for each walker. Further, our prior work on occupant tracking could be leveraged to remove the assumptions of alternating feet by determining the walking direction and relative location of each step (Pan et al. 2014). In this way, the system could determine which foot each step belongs to and automatically cluster it into the appropriate cluster for the right or left foot.

Conclusions

To the best of our knowledge, this paper represents the first work that utilizes footstep-induced vibration sensing to estimate walking gait balance symmetry and footstep ground reaction forces. We utilize floor vibrations due to their ability to sense footsteps in a passive manner and with sparse deployment. We overcome system challenges of the *structural variation effect* and *gait sampling bias* on the footstep GRF-vibration signal amplitude relationship by modeling variations in the underlying structure through an unsupervised PCA-based clustering approach and through a kernel-based robust regression. Then, using consecutive pairs of footstep ground reaction force estimations, we estimate gait balance symmetry using a common metric known as the symmetry index. Our experimental evaluation explored the robustness of our method with respect to varying structural conditions, walking speed/balance conditions, and different individuals (i.e., walking styles). Through this evaluation, our approach realizes an overall force estimation accuracy of up to 92% (1.5X improvement over the baseline approach) and a trace-level balance SI estimation accuracy as high as 96.5% (2.2X baseline improvement). The results from our work are promising and show that this technique has the potential for gait monitoring in a variety of indoor and home-health care settings.

Data Availability Statement

Some or all data, models, or code generated or used during the study are proprietary or confidential in nature and may only be provided with restrictions. Specifically, anonymized raw vibration and pressure sensor data is available upon request.

Acknowledgments

This research was partially supported by the National Science Foundation (NSF) Career (CMMI-2026699), Google, Intel, and Highmark. The authors would also like to acknowledge Baptist Homes and Vincentian Homes for providing insight into gait analysis and for providing deployment sites for data collection and analysis.

References

Alajlouni, S., M. Albakri, and P. Tarazaga. 2018. "Impact localization in dispersive waveguides based on energy-attenuation of waves with the traveled distance." *Mech. Syst. Sig. Process.* 105 (May): 361–376. https://doi.org/10.1016/j.ymssp.2017.12.007.

Aruin, A. S., and N. Kanekar. 2013. "Effect of a textured insole on balance and gait symmetry." *Exp. Brain Res.* 231 (2): 201–208. https://doi.org/10.1007/s00221-013-3685-z.

Baron, M. 2013. *Probability and statistics for computer scientists*. Boca Raton, FL: CRC Press.

Benedetti, M. G., R. Piperno, L. Simoncini, P. Bonato, A. Tonini, and S. Giannini. 1999. "Gait abnormalities in minimally impaired multiple sclerosis patients." *Multiple Sclerosis J.* 5 (5): 363–368. https://doi.org/10.1177/135245859900500510.

Berg, K., S. Wood-Dauphine, J. Williams, and D. Gayton. 1989. "Measuring balance in the elderly: Preliminary development of an instrument." *Physiother. Can.* 41 (6): 304–311. https://doi.org/10.3138/ptc.41.6.304.

Bonde, A., S. Pan, M. Mirshekari, C. Ruiz, H. Y. Noh, and P. Zhang. 2020. "OAC: Overlapping office activity classification through IoT-sensed structural vibration." In *Proc., IEEE/ACM 5th Int. Conf. on Internet-of-Things Design and Implementation*, 216–222. New York: IEEE.

Bowman, A. W., and A. Azzalini. 1997. Vol. 18 of *Applied smoothing techniques for data analysis: The kernel approach with S-plus illustrations*. Oxford, UK: OUP Oxford.

Browne, J., and N. O'Hare. 2001. "Review of the different methods for assessing standing balance." *Physiotherapy* 87 (9): 489–495. https://doi.org/10.1016/S0031-9406(05)60696-7.

Calfa, B., I. Grossmann, A. Agarwal, S. Bury, and J. Wassick. 2015. "Data-driven individual and joint chance-constrained optimization via kernel smoothing." *Comput. Chem. Eng.* 78 (Jul): 51–69. https://doi.org/10.1016/j.compchemeng.2015.04.012.

Cao, X., Y. Sugiyama, and Y. Mitsui. 1998. "Application of artificial neural networks to load identification." *Comput. Struct.* 69 (1): 63–78. https://doi.org/10.1016/S0045-7949(98)00085-6.

Dong, Y., J. J. Zou, J. Liu, J. Fagert, M. Mirshekari, L. Lowes, M. Iammarino, P. Zhang, and H. Y. Noh. 2020. "MD-Vibe: Physics-informed analysis of patient-induced structural vibration data for monitoring gait health in individuals with muscular dystrophy." In *Proc., UbiComp/ISWC '20: Adjunct Proc., 2020 ACM Int. Joint Conf. on Pervasive and Ubiquitous Computing and Proc., 2020 ACM Int. Symp. on Wearable Computers*, 525–531. Los Alamitos, CA: IEEE Computer Society.

Drira, S., Y. Reuland, N. F. Olsen, S. G. Pai, and I. F. Smith. 2019. "Occupant-detection strategy using footstep-induced floor vibrations." In *Proc., 1st ACM Int. Workshop on Device-Free Human Sensing*, 31–34. New York: Association for Computing Machinery.

Fagert, J., M. Mirshekari, S. Pan, P. Zhang, and H. Y. Noh. 2017a. "Characterizing left-right gait balance using footstep-induced structural vibrations." In Vol. 10168 of *Proc., Sensors and Smart Structures Technologies for Civil, Mechanical, and Aerospace Systems*, 10168–10168. Bellingham WA: International Society for Optics and Photonics.

Fagert, J., M. Mirshekari, S. Pan, P. Zhang, and H. Y. Noh. 2019a. "Characterizing structural changes to estimate walking gait balance." In Vol. 2 of *Proc., Dynamics of Civil Structures*, 333–335. Cham, Switzerland: Springer.

Fagert, J., M. Mirshekari, S. Pan, P. Zhang, and H. Y. Noh. 2019b. "Gait health monitoring through footstep-induced floor vibrations." In *Proc., 18th ACM/IEEE Int. Conf. on Information Processing in Sensor Networks*, 319–320. New York: IEEE.

Fagert, J., M. Mirshekari, S. Pan, P. Zhang, and H. Y. Noh. 2020. "Structural property guided gait parameter estimation using footstep-induced floor vibrations." In Vol. 2 of *Proc., Dynamics of Civil Structures*, edited by S. Pakzad, 191–194. Cham, Switzerland: Springer.

Fagert, J., M. Mishekari, S. Pan, P. Zhang, and H. Y. Noh. 2017b. "Monitoring hand-washing practices using structural vibrations." In *Proc., Structural Health Monitoring 2017*. Lancaster, PA: DEStech Publications.

Fagert, J., M. Mishekari, S. Pan, P. Zhang, and H. Y. Noh. 2019c. "Vibration source separation for multiple people gait monitoring using footstep-induced floor vibrations." In *Proc., Structural Health Monitoring 2019*. Lancaster, PA: DEStech Publications.

Gabel, M., R. Gilad-Bachrach, E. Renshaw, and A. Schuster. 2012. "Full body gait analysis with Kinect." In *Proc., Annual Int. Conf. of the IEEE Engineering in Medicine and Biology Society*, 1964–1967. New York: IEEE.

Gingrich, P. 1992. *Introductory statistics for the social sciences*. Regina, SK: Dept. of Sociology and Social Sciences, Univ. of Regina.

Gutierrez-Farewik, E. M., Å. Bartonek, and H. Saraste. 2006. "Comparison and evaluation of two common methods to measure center of mass displacement in three dimensions during gait." *Hum. Mov. Sci.* 25 (2): 238–256. https://doi.org/10.1016/j.humov.2005.11.001.

Herzog, W. A., B. M. Nigg, L. J. Read, and E. Olsson. 1989. "Asymmetries in ground reaction force in normal human gait." *Med. Sci. Sports Exercise* 21 (1): 110–114. https://doi.org/10.1249/00005768-198902000-00020.

Hodt-Billington, C., J. L. Helbostad, W. Vervaat, T. Rognsvåg, and R. Moe-Nilssen. 2012. "Criteria of gait asymmetry in patients with hip osteoarthritis." *Physiother. Theory Pract.* 28 (2): 134–141. https://doi.org/10.3109/09593985.2011.574783.

Hof, A., M. Gazendam, and W. Sinke. 2005. "The condition for dynamic stability." *J. Biomech.* 38 (1): 1–8. https://doi.org/10.1016/j.jbiomech.2004.03.025.

Horak, F. B. 1997. "Clinical assessment of balance disorders." *Gait Posture* 6 (1): 76–84. https://doi.org/10.1016/S0966-6362(97)00018-0.

I/O Sensor Nederland bv. 2006. *SM-24 geophone element*. P/N 1004117. Stafford, TX: I/O Sensor Nederland bv.

Jolliffe, I. 2002. *Principal component analysis*. 2nd ed. New York: Springer.

Jonsdottir, J., and D. Cattaneo. 2007. "Reliability and validity of the dynamic gait index in persons with chronic stroke." *Arch. Phys. Med. Rehabil.* 88 (11): 1410–1415. https://doi.org/10.1016/j.apmr.2007.08.109.

Kamen, G., C. Patten, C. Du, and S. Sison. 1998. "An accelerometry-based system for the assessment of balance and postural sway." *Gerontology* 44 (1): 40–45. https://doi.org/10.1159/000021981.

Karuka, A. H., J. A. M. G. Silva, and M. T. Navega. 2011. "Analysis of agreement of assessment tools of body balance in the elderly." [In Portuguese.] *Braz. J. Phys. Ther.* 15 (6): 460–466. https://doi.org/10.1590/S1413-35552011000600006.

Kelly, S. G. 2012. *Mechanical vibrations: Theory and applications*. Stamford, CT: Cengage Learning.

Kessler, E., V. V. S. Malladi, and P. A. Tarazaga. 2019. "Vibration-based gait analysis via instrumented buildings." *Int. J. Distrib. Sens. Netw.* 15 (10): 1550147719881608. https://doi.org/10.1177/1550147719881608.

Lam, M., M. Mirshekari, S. Pan, P. Zhang, and H. Y. Noh. 2016. "Robust occupant detection through step-induced floor vibration by incorporating structural characteristics." In Vol. 4 of *Proc., Dynamics of Coupled Structures*, 357–367. Cham, Switzerland: Springer.

Law, S. 2002. "Dynamic load from pedestrian footsteps." In *Proc., Advances in Steel Structures (ICASS '02)*, edited by S. Chan, J. Teng, and K. Chung, 905–912. Oxford, UK: Elsevier.

Lee, Y. H., and T. Oh. 2016. "The simple lamb wave analysis to characterize concrete wide beams by the practical MASW test." *Materials* 9 (6): 437. https://doi.org/10.3390/ma9060437.

Little, R. J. A., and D. B. Rubin. 2019. *Statistical analysis with missing data*. Hoboken, NJ: Wiley.

Lord, M., D. P. Reynolds, and J. R. Hughes. 1986. "Foot pressure measurement: A review of clinical findings." *J. Biomed. Eng.* 8 (4): 283–294. https://doi.org/10.1016/0141-5425(86)90060-9.

Lord, S. R., H. B. Menz, and A. Tiedemann. 2003. "A physiological profile approach to falls risk assessment and prevention." *Phys. Ther.* 83 (3): 237. https://doi.org/10.1093/ptj/83.3.237.

Lugade, V., and K. Kaufman. 2014. "Dynamic stability margin using a marker based system and Tekscan: A comparison of four gait conditions." *Gait Posture* 40 (1): 252–254. https://doi.org/10.1016/j.gaitpost.2013.12.023.

Lugade, V., V. Lin, and L.-S. Chou. 2011. "Center of mass and base of support interaction during gait." *Gait Posture* 33 (3): 406–411. https://doi.org/10.1016/j.gaitpost.2010.12.013.

MacQueen, J. 1967. "Some methods for classification and analysis of multivariate observations." In Vol. 1 of *Proc., 5th Berkeley Symp. on Mathematical Statistics and Probability*, 281–297. Berkeley, CA: University of California Press.

Madarshahian, R., J. M. Caicedo, and D. A. Zambrana. 2016. "Benchmark problem for human activity identification using floor vibrations." *Expert Syst. Appl.* 62 (Nov): 263–272. https://doi.org/10.1016/j.eswa.2016.06.027.

Mancini, M., and F. B. Horak. 2010. "The relevance of clinical balance assessment tools to differentiate balance deficits." *Eur. J. Phys. Rehab. Med.* 46 (2): 239–248.

Mathias, S., U. S. Nayak, and B. Isaacs. 1986. "Balance in elderly patients: The 'get-up and go' test." *Arch. Phys. Med. Rehab.* 67 (6): 387.

McDonough, A. L., M. Batavia, F. C. Chen, S. Kwon, and J. Ziai. 2001. "The validity and reliability of the GAITRite system's measurements: A preliminary evaluation." *Arch. Phys. Med. Rehab.* 82 (3): 419–425. https://doi.org/10.1053/apmr.2001.19778.

Mirshekari, M., J. Fagert, A. Bonde, P. Zhang, and H. Y. Noh. 2018a. "Human gait monitoring using footstep-induced floor vibrations across different structures." In *Proc., ACM Int. Joint Conf. and 2018 Int. Symp. on Pervasive and Ubiquitous Computing and Wearable Computers*, 1382–1391. New York: Association for Computing Machinery.

Mirshekari, M., J. Fagert, S. Pan, P. Zhang, and H. Y. Noh. 2020. "Step-level occupant detection across different structures through footstep-induced floor vibration using model transfer." *J. Eng. Mech.* 146 (3): 04019137. https://doi.org/10.1061/(ASCE)EM.1943-7889.0001719.

Mirshekari, M., S. Pan, J. Fagert, E. M. Schooler, P. Zhang, and H. Y. Noh. 2018b. "Occupant localization using footstep-induced structural vibration." *Mech. Syst. Sig. Process.* 112 (Nov): 77–97. https://doi.org/10.1016/j.ymssp.2018.04.026.

Mirshekari, M., S. Pan, P. Zhang, and H. Y. Noh. 2016. "Characterizing wave propagation to improve indoor step-level person localization using floor vibration." In Vol. 9803 of *Proc., Sensors and Smart Structures Technologies for Civil, Mechanical, and Aerospace Systems 2016*, 980305. Bellingham WA: International Society for Optics and Photonics.

Muro-de-la Herran, A., B. Garcia-Zapirain, and A. Mendez-Zorrilla. 2014. "Gait analysis methods: An overview of wearable and non-wearable systems, highlighting clinical applications." *Sensors* 14 (2): 3362–3394. https://doi.org/10.3390/s140203362.

Nevitt, M. C., S. R. Cummings, S. Kidd, and D. Black. 1989. "Risk factors for recurrent nonsyncopal falls: A prospective study." *J. Am. Med. Assoc.* 261 (18): 2663–2668. https://doi.org/10.1001/jama.1989.03420180087036.

Noh, H. Y., D. Lallemant, and A. S. Kiremidjian. 2015. "Development of empirical and analytical fragility functions using kernel smoothing methods." *Earthquake Eng. Struct. Dyn.* 44 (8): 1163–1180. https://doi.org/10.1002/eqe.2505.

Noh, H. Y., D. G. Lignos, K. K. Nair, and A. S. Kiremidjian. 2012. "Development of fragility functions as a damage classification/prediction method for steel moment-resisting frames using a wavelet-based damage sensitive feature." *Earthquake Eng. Struct. Dyn.* 41 (4): 681–696. https://doi.org/10.1002/eqe.1151.

Pai, S. G., Y. Reuland, S. Drira, and I. F. Smith. 2019. "Is there a relationship between footstep-impact locations and measured signal characteristics?" In *Proc., 1st ACM Int. Workshop on Device-Free Human Sensing*, 62–65. New York: Association for Computing Machinery.

Pan, S., M. Berges, J. Rodakowski, P. Zhang, and H. Y. Noh. 2019. "Fine-grained recognition of activities of daily living through structural vibration and electrical sensing." In *Proc., 6th ACM Int. Conf. on Systems for Energy-Efficient Buildings, Cities, and Transportation*, 149–158. New York: Association for Computing Machinery.

Pan, S., A. Bonde, J. Jing, L. Zhang, P. Zhang, and H. Y. Noh. 2014. "BOES: Building occupancy estimation system using sparse ambient vibration monitoring." In Vol. 9061 of *Proc., Sensors and Smart Structures Technologies for Civil, Mechanical, and Aerospace Systems 2014*, 906110. Bellingham WA: International Society for Optics and Photonics.

Pan, S., K. Lyons, M. Mirshekari, H. Y. Noh, and P. Zhang. 2016. "Multiple pedestrian tracking through ambient structural vibration sensing." In *Proc., 14th ACM Conf. on Embedded Network Sensor Systems CD-ROM*, 366–367. New York: Association for Computing Machinery.

Pan, S., M. Mirshekari, J. Fagert, C. G. Ramirez, A. J. Chung, C. C. Hu, J. P. Shen, P. Zhang, and H. Y. Noh. 2018. "Characterizing human activity induced impulse and slip-pulse excitations through structural vibration." *J. Sound Vib.* 414 (Feb): 61–80. https://doi.org/10.1016/j.jsv.2017.10.034.

Pan, S., C. G. Ramirez, M. Mirshekari, J. Fagert, A. J. Chung, C. C. Hu, J. P. Shen, H. Y. Noh, and P. Zhang. 2017a. "Surfacevibe: Vibration-based tap & swipe tracking on ubiquitous surfaces." In *Proc., 16th ACM/IEEE Int. Conf. on Information Processing in Sensor Networks*, 208–197. New York: IEEE.

Pan, S., N. Wang, Y. Qian, I. Velibeyoglu, H. Y. Noh, and P. Zhang. 2015. "Indoor person identification through footstep induced structural vibration." In *Proc., 16th Int. Workshop on Mobile Computing Systems and Applications*, 81–86. New York: Association for Computing Machinery.

Pan, S., S. Xu, M. Mirshekari, P. Zhang, and H. Y. Noh. 2017b. "Collaboratively adaptive vibration sensing system for high-fidelity monitoring of structural responses induced by pedestrians." *Front. Built Environ.* 3 (May): 28. https://doi.org/10.3389/fbuil.2017.00028.

Pan, S., T. Yu, M. Mirshekari, J. Fagert, A. Bonde, O. J. Mengshoel, H. Y. Noh, and P. Zhang. 2017c. "Footprintid: Indoor pedestrian identification through ambient structural vibration sensing." *Proc. ACM Interact. Mobile Wearable Ubiquitous Technol.* 1 (3): 1. https://doi.org/10.1145/3130954.

Pardasaney, P. K., N. K. Latham, A. M. Jette, R. C. Wagenaar, P. Ni, M. D. Slavin, and J. F. Bean. 2012. "Sensitivity to change and responsiveness of four balance measures for community-dwelling older adults." *Phys. Ther.* 92 (3): 388–397. https://doi.org/10.2522/ptj.20100398.

Patel, M. S., D. A. Asch, and K. G. Volpp. 2015. "Wearable devices as facilitators, not drivers, of health behavior change." *J. Am. Med. Assoc.* 313 (5): 459–460. https://doi.org/10.1001/jama.2014.14781.

Perell, K. L., A. Nelson, R. L. Goldman, S. L. Luther, N. Prieto-Lewis, and L. Z. Rubenstein. 2001. "Fall risk assessment measures: An analytic review." *J. Gerontology Ser. A* 56 (12): 761–766. https://doi.org/10.1093/gerona/56.12.M761.

Peters, M. 1988. "Footedness: Asymmetries in foot preference and skill and neuropsychological assessment of foot movement." *Psychol. Bull.* 103 (2): 179–192. https://doi.org/10.1037/0033-2909.103.2.179.

Pimentel, R., A. Pavic, and P. Waldron. 2001. "Evaluation of design requirements for footbridges excited by vertical forces from walking." *Can. J. Civ. Eng.* 28 (5): 769–777. https://doi.org/10.1139/l01-036.

Poston, J. D., R. M. Buehrer, and P. A. Tarazaga. 2017a. "A framework for occupancy tracking in a building via structural dynamics sensing of footstep vibrations." *Front. Built Environ.* 3 (Nov): 65. https://doi.org/10.3389/fbuil.2017.00065.

Poston, J. D., R. M. Buehrer, and P. A. Tarazaga. 2017b. "Indoor footstep localization from structural dynamics instrumentation." *Mech. Syst. Sig. Process.* 88 (May): 224–239. https://doi.org/10.1016/j.ymssp.2016.11.023.

Racic, V., and J. Brownjohn. 2011. "Stochastic model of near-periodic vertical loads due to humans walking." *Adv. Eng. Inf.* 25 (2): 259–275. https://doi.org/10.1016/j.aei.2010.07.004.

Racic, V., A. Pavic, and J. Brownjohn. 2009. "Experimental identification and analytical modelling of human walking forces: Literature review." *J. Sound Vib.* 326 (1): 1–49. https://doi.org/10.1016/j.jsv.2009.04.020.
Racine, J. S. 2008. *Nonparametric econometrics: A primer*. Boston: Now Publishers.
Rousseeuw, P. J., and A. M. Leroy. 2005. Vol. 589 of *Robust regression and outlier detection*. New York: Wiley.
Rubenstein, L. Z. 2006. "Falls in older people: Epidemiology, risk factors and strategies for prevention." Supplement, *Age Ageing* 35 (S2): 37–41. https://doi.org/10.1093/ageing/afl084.
Sadeghi, H., P. Allard, F. Prince, and H. Labelle. 2000. "Symmetry and limb dominance in able-bodied gait: A review." *Gait Posture* 12 (1): 34–45. https://doi.org/10.1016/S0966-6362(00)00070-9.
Samson, M., A. Crowe, P. De Vreede, J. Dessens, S. Duursma, and H. Verhaar. 2001. "Differences in gait parameters at a preferred walking speed in healthy subjects due to age, height and body weight." *Aging Clin. Exp. Res.* 13 (1): 16–21. https://doi.org/10.1007/BF03351489.
Shahabpoor, E., A. Pavic, and V. Racic. 2016. "Identification of mass–spring–damper model of walking humans." *Structures* 5 (Feb): 233–246. https://doi.org/10.1016/j.istruc.2015.12.001.
Shi, L., M. Mirshekari, J. Fagert, Y. Chi, H. Y. Noh, P. Zhang, and S. Pan. 2019. "Device-free multiple people localization through floor vibration." In *Proc., 1st ACM Int. Workshop on Device-Free Human Sensing*, 57–61. New York: Association for Computing Machinery.
Shumway-Cook, A., and M. H. Woollacott. 1995. *Motor control: Theory and practical applications*. Baltimore: Williams and Wilkins.
Shupert, C., and F. Horak. 2016. *Balance and falls in the older adult*. Rep. No. Portland, OR: Vestibular Disorders Association.
Spain, R., R. St George, A. Salarian, M. Mancini, J. Wagner, F. Horak, and D. Bourdette. 2012. "Body-worn motion sensors detect balance and gait deficits in people with multiple sclerosis who have normal walking speed." *Gait Posture* 35 (4): 573–578. https://doi.org/10.1016/j.gaitpost.2011.11.026.
Stein, S., and M. Wysession. 2009. *An introduction to seismology, earthquakes, and earth structure*. New York: Wiley.
Tekscan. 2010. *Flexiforce sensors users manual*. Boston: Tekscan.
Tien, I., S. D. Glaser, and M. J. Aminoff. 2010. "Characterization of gait abnormalities in Parkinson's disease using a wireless inertial sensor system." In *Proc., Annual Int. Conf. of the IEEE Engineering in Medicine and Biology Society*, 3353–3356. New York: IEEE.
Tudor-Locke, C., S. M. Camhi, C. Leonardi, W. D. Johnson, P. T. Katzmarzyk, C. P. Earnest, and T. S. Church. 2011. "Patterns of adult stepping cadence in the 2005–2006 NHANES." *Preventive Med.* 53 (3): 178–181. https://doi.org/10.1016/j.ypmed.2011.06.004.
Uustal, H., and E. Baerga. 2004. *Physical medicine and rehabilitation board review*. 3rd ed. New York: Demos Medical Publishing.
van Meulen, F. B., D. Weenk, J. H. Buurke, B.-J. F. van Beijnum, and P. H. Veltink. 2016a. "Ambulatory assessment of walking balance after stroke using instrumented shoes." *J. NeuroEng. Rehabil.* 13 (1): 48. https://doi.org/10.1186/s12984-016-0146-5.
van Meulen, F. B., D. Weenk, E. H. van Asseldonk, H. M. Schepers, P. H. Veltink, and J. H. Buurke. 2016b. "Analysis of balance during functional walking in stroke survivors." *PLoS One* 11 (11): 1–20. https://doi.org/10.1371/journal.pone.0166789.
Vaught, S. L. 2001. "Gait, balance, and fall prevention." *Ochsner J.* 3 (2): 94–97.
Verdini, F., M. Marcucci, M. Benedetti, and T. Leo. 2006. "Identification and characterisation of heel strike transient." *Gait Posture* 24 (1): 77–84. https://doi.org/10.1016/j.gaitpost.2005.07.008.
Wafai, L., A. Zayegh, J. Woulfe, S. M. Aziz, and R. Begg. 2015. "Identification of foot pathologies based on plantar pressure asymmetry." *Sensors* 15 (8): 20392–20408. https://doi.org/10.3390/s150820392.
Wearing, S. C., S. R. Urry, and J. E. Smeathers. 2001. "Ground reaction forces at discrete sites of the foot derived from pressure plate measurements." *Foot Ankle Int.* 22 (8): 653–661. https://doi.org/10.1177/107110070102200807.
Whittle, M. W. 1999. "Generation and attenuation of transient impulsive forces beneath the foot: A review." *Gait Posture* 10 (3): 264–275. https://doi.org/10.1016/S0966-6362(99)00041-7.
Willford, M., C. Field, and P. Young. 2006. "Improved methodologies for the prediction of footfall-induced vibration." In Vol. 5933 of *Proc. Building Integration Solutions*, 1–15. Reston, VA: ASCE.
Worden, K. 2001. "Rayleigh and lamb waves-basic principles." *Strain* 37 (4): 167–172. https://doi.org/10.1111/j.1475-1305.2001.tb01254.x.
Xue, Z., D. Ming, W. Song, B. Wan, and S. Jin. 2010. "Infrared gait recognition based on wavelet transform and support vector machine." *Pattern Recognit.* 43 (8): 2904–2910. https://doi.org/10.1016/j.patcog.2010.03.011.
Živanović, S., A. Pavić, and P. Reynolds. 2007. "Probability-based prediction of multi-mode vibration response to walking excitation." *Eng. Struct.* 29 (6): 942–954. https://doi.org/10.1016/j.engstruct.2006.07.004.